Interannual variability of spring and summer monsoon growing season carbon exchange at a semiarid savanna over nearly two decades

Russell L. Scott[1], Miriam R. Johnston[2], John F. Knowles[3], Natasha MacBean[4,5], Kashif Mahmud[6], Matt C. Roby[7], Matthew P. Dannenberg[2]

[1]Southwest Watershed Research Center, USDA-ARS, 2000 E. Allen Road, Tucson, Arizona USA 85716

[2]Department of Geographical and Sustainability Sciences, University of Iowa, Iowa City, IA 52242

[3]Department of Earth and Environmental Sciences, California State University, Chico, Chico, CA 95929

[4]Department of Geography and Environment, Western University, London, ON, N6A 5C2, Canada

[5]Department of Biology, Western University, London, ON, N6A 3K7, Canada

[6]Kimbell School of Geosciences, Midwestern State University, Wichita Falls, TX 76308

[7]Sustainable Agricultural Water Systems Research Unit, USDA-ARS, Davis, CA 95616

Corresponding author: Russell Scott, Southwest Watershed Research Center, USDA-ARS, 2000 E. Allen Road, Tucson, Arizona USA 85719. Email: russ.scott@usda.gov

Keywords: Carbon, Water, Ecosystem, Eddy covariance, Dryland, Remote Sensing, Gross Primary Production, GPP

Highlights

- Large interannual variability of ecosystem carbon fluxes at a semiarid savanna site
- Flux variability governed by water availability metrics like precipitation and soil moisture
- Positive trend in 19-year soil moisture and carbon uptake record
- Models and satellites often capture less than half the variability in measured fluxes

Abstract

Eddy covariance measurements of land-atmosphere energy, carbon, and water exchange now span multiple decades at some sites, supporting an improved understanding of flux interannual variability (IAV) and its ecophysiological and physical controls. Most eddy covariance IAV studies have focused on temperate forest ecosystems, where carbon fluxes are large and flux records are longest – but also where IAV is much lower than in dryland regions, which have been identified as an essential driver of the trend and variability in the global terrestrial carbon sink. In this study, we leveraged 19 years of continuous micrometeorological measurements at the AmeriFlux US-SRM mesquite savanna site in southern Arizona, USA to quantify the IAV, trends, and drivers of carbon fluxes during the distinct spring and summer growing seasons. We also assessed the ability of modern satellite and land surface models to capture the IAV of seasonal water and carbon fluxes. Annual net ecosystem production (NEP) was small and highly variable (23 +/- 64 gC m^{-2} yr^{-1}). Precipitation and associated measures of water availability determined most of the variability in NEP, largely through their influence on annual and seasonal gross ecosystem productivity (GEP) as opposed to ecosystem respiration (ER). Root-zone soil moisture captured between 73% (spring) and 85% (summer) of GEP variability and between 73% (spring) and 58% (summer) of ER variability. Throughout the study period, soil moisture and greenness increased with associated increases in GEP, ER and NEP. These trends were strongly influenced by very productive and wet summer growing seasons during the last two years, which were characterized by abundant understory grass cover. Typically, less than half of the variability in growing season GEP and evapotranspiration was captured by satellite-based estimates and land surface model simulations with local site forcing and calibration, highlighting the ongoing utility of long-term datasets to support careful model testing and improvement.

1. Introduction

Drylands, classified as arid, semiarid, or subhumid, are defined as regions with high aridity where potential evaporation exceeds precipitation for much of the year (Jenerette et al., 2012; Poulter et al., 2014). Though low water availability limits the magnitude of carbon stocks and fluxes in drylands relative to more humid regions, drylands play a dominant role in the trend and interannual variability (IAV) of the global land carbon sink because their productivity is closely coupled to environmental conditions, and they cover about 40% of the Earth's terrestrial surface (Ahlström et al., 2015; Humphrey et al., 2021; Poulter et al., 2014). Specifically, carbon flux variability tends to increase with site dryness (Baldocchi et al., 2018; Biederman et al., 2017) as a result of increasing correlation with water availability, which is typically more variable than the dominant controls on carbon exchange in more mesic ecosystems. Furthermore, drylands are warming more rapidly than other regions (Huang et al., 2017; L. Zhou et al., 2015); it is therefore vital to monitor dryland carbon and water fluxes and their drivers with in-situ measurements as a means to assess and improve satellite and land surface models of carbon and water exchange (Prentice et al., 2015; Running et al., 1999). Direct measurements of dryland ecosystem fluxes using the eddy covariance method are an essential component of this task (Baldocchi, 2003), along with data collation, standardization, and sharing networks like AmeriFlux (Novick et al., 2018 and highlighted in this special issue), OzFlux (Beringer et al., 2022) and FLUXNET (Pastorello et al., 2020).

Continuous ecosystem flux measurements began in the 1980s and 1990s with the advent of improved measurement equipment like smaller computers, sonic anemometers, and trace gas analyzers (Baldocchi et al., 1988; Goulden et al., 1996; Shuttleworth, 1988). Associated flux site networks like AmeriFlux coalesced in the 1990s, focused primarily on forested sites with temperate climates, as these were geographically proximal to most flux researchers and represented large gross carbon fluxes (Novick et al., 2018). At this time, drylands received very limited attention (Hastings et al., 2005; Hutley et al., 2000; Unland et al., 1996), likely due to lack of funding and the widespread impression that they were irrelevant to the global carbon cycle. Consequently, measurement of fluxes from dryland sites lagged measurement of fluxes from more mesic sites by about a decade in the Americas (Fig. 1, left), despite drylands making up roughly 30% of the AmeriFlux domain (North and South America). While there are now multiple mesic forested and woodland sites with greater than two decades of data, only five

dryland sites in the AmeriFlux repository have 10-15 years of archived data, and only two have 16-20 years (Fig. 1, right).

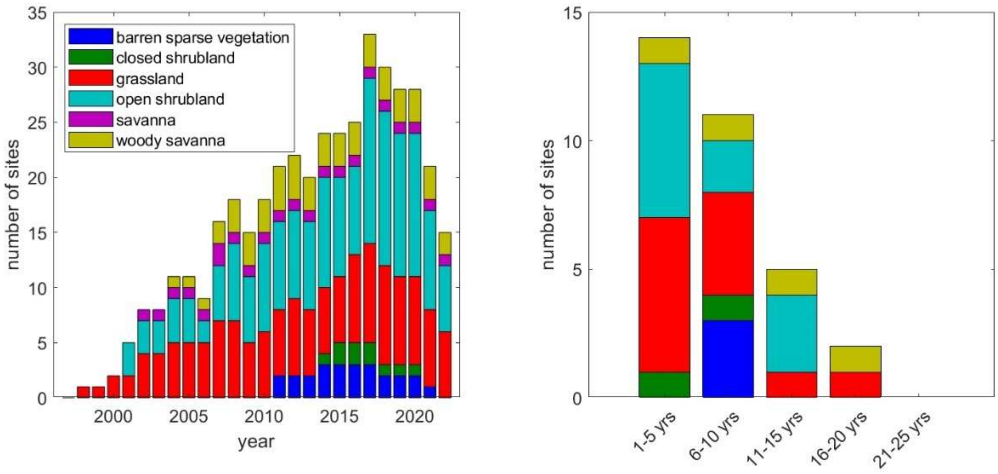

Figure 1. Number of dryland AmeriFlux sites by International Geosphere–Biosphere Programme (IGBP) category, with data availability by year and by record length. Results are from an AmeriFlux site search (https://ameriflux.lbl.gov/, accessed Nov. 20, 2022), with the following criteria: 1) mean annual precipitation < 500 mm yr^{-1}, 2) excluding cropland, forest and wetland IGBP cover types. The drop-off in data availability after 2017 is likely due to a lag between data collection and site operator submission to the AmeriFlux network.

Robust examination of dryland carbon and water IAV and its drivers is a priority because atmospheric inversions of net carbon dioxide (CO_2) show substantial variation in the dryland terrestrial carbon sink (Poulter et al., 2014; Zhang et al., 2018), and climate change is inducing trends in the drivers of water and carbon fluxes (Ficklin and Novick, 2017; Friedlingstein et al., 2022). Furthermore, satellite and land surface models (LSMs) within Earth system models often underestimate IAV (Keenan et al., 2012; MacBean et al., 2021). To better understand the interannual variability and trends of dryland carbon fluxes and their drivers, we used data from one of the longest dryland data records: a semiarid savanna site in southern Arizona, USA. This site is located in the northern part of the North American Monsoon region (Adams and Comrie, 1997) and is thus characterized by a dominant warm summer growing season as well as a subdominant spring growing season in years with sufficient late fall/winter precipitation.

Using 19 years of continuous eddy covariance, soil, and meteorological measurements, our objectives were to: 1) Investigate coupling between the interannual variability of hydrometeorological drivers and ecosystem carbon fluxes, 2) Quantify trends in hydrometeorological drivers and ecosystem carbon fluxes during both the spring and summer growing seasons, and 3) Assess the ability of modern land surface and satellite models to reproduce the IAV of carbon and water fluxes at this site. While our results are limited to one location, the magnitude and seasonal patterns of the site's average water and carbon exchange are similar to other semiarid shrubland and grassland sites in the Sonoran and Chihuahuan desert regions of the greater North American Monsoon region (Anderson-Teixeira et al., 2011; Biederman et al., 2017; Pérez-Ruiz et al., 2022; Scott et al., 2015) as well as to other warm dryland sites that receive precipitation mainly in summer (e.g., parts of Australia, southern and Sahel regions of Africa). Therefore, these results have broad implications for other semiarid savannas, grasslands and shrublands.

2. Site Description, Climatology, and Expected Results

We used data collected from 2004 through 2022 at the Santa Rita Mesquite Savanna (Scott et al., 2009) (AmeriFlux site US-SRM, 31.822N, 110.867W, elevation: 1116 m). The site has a mix of low-statured trees with an understory of grasses, sub-shrubs, and succulents. The tree cover fraction, consisting mainly of velvet mesquite (*Prosopis velutina*), is ~30%, which is at the margin of the IGBP biome classifications for savanna (SAV) and woody savanna (WSA). While mesquite is a facultative phreatophyte, there is no evidence that the trees access groundwater at this site where the water table is very deep (Potts et al., 2008). Perennial C4 bunchgrass and annual (*Aristida spp., Digitaria californica, Muhlenbergia porteri, Bouteloua eriopoda, Eragrostis lehmanniana, Bouteloua aristidoides*) cover ranges from 15-60% depending on summer rainfall, and scattered sub-shrub and succulent cover fractions are low (Vivoni et al., 2022). The bare soil fraction (20-50%) supports annual grasses and forbs when rainfall is sufficient. Soils are deep loamy sand. Principal topics for previous studies using flux data at this site include woody plant encroachment (Scott et al., 2015; Vivoni et al., 2022), tree versus grass competition (Barron-Gafford et al., 2017; Potts et al., 2008), ecohydrology and hydraulic redistribution (Lee et al., 2018; Scott et al., 2008; Scott and Biederman, 2019), soil respiration (Barba et al., 2018; Cable et al., 2012; Roby et al., 2019), carbon cycling (Biederman et al., 2017), and plant ecophysiology (Barron-Gafford et al., 2013; Hamerlynck et al., 2012, 2010). In the following section, we set the stage for the current study's hypotheses and results concerning the interannual variability of the savanna's two growing seasons by reviewing the seasonality of the site's hydrometeorology and carbon fluxes.

With 19-years of data, we can define an increasingly robust hydrometeorological and carbon flux characterization of the site. The climate at US-SRM is classified as semiarid and monsoonal with about 55% of the annual precipitation falling in the warm summer months of July through September and approximately 30% in the more hydrologically variable and cooler winter months of November-February (Fig. 2). The foresummer months of May-June were reliably hot and dry while precipitation in the fall months of September and October was occasionally augmented by tropical disturbances. The seasonality of precipitation and air temperature gave rise to bimodal patterns of soil volumetric water content (VWC) and plant greenness (as quantified by the Enhanced Vegetation Index, EVI, Fig. 2). Soil moisture peaked in winter when atmospheric and plant water demand was low, declined to the annual minimum in the foresummer, then increased again during the monsoon before decreasing in the fall (though not as completely or reliably as in the foresummer). Legacy VWC from wet fall periods sometimes persisted until spring. Soil water in the 0-30 cm rootzone for many of the understory plants (mainly grasses) dried faster and more profoundly than 0-130 cm soil water, which was likely more representative of the deeper soil volume accessible to overstory trees. Spring green-up was dominated by mesquite trees leafing out in early April regardless of winter/spring precipitation, whereas increased summer greening was due to understory grasses and, occasionally, additional mesquite leaf-flush in years with abundant precipitation (Steiner, 2022). In the fall, greenness decreased as most understory grasses began to brown in September, whereas mesquite trees retained their leaves until the cold winter storms.

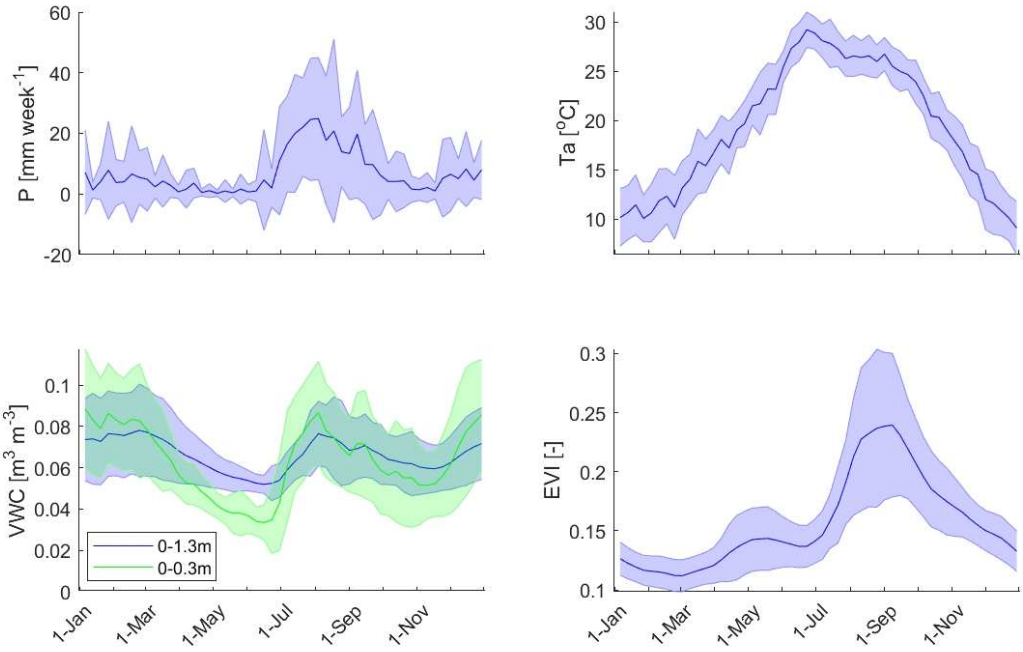

Figure 2. The 2004-2022 weekly mean (+/- 1 standard deviation) precipitation (P), air temperature (Ta), soil volumetric water content (VWC) at 0-1.3 m and 0-0.3 m depths, and MODIS enhanced vegetation index (EVI).

The seasonality of site meteorology and plant phenology led to bimodal patterns of land-atmosphere CO_2 and water exchanges (Fig. 3). The average net CO_2 uptake (NEP) tended to be slightly negative from November through April and positive for a shorter spring and longer summer period. Bimodality was strongest for gross ecosystem productivity (GEP) with clear spring and summer peaks, whereas peaks in ecosystem respiration (ER) were less pronounced and broader. Evapotranspiration (ET) seasonality was more unimodal, like ER, but less reduced in winter. GEP peaks lagged 1-2 weeks behind both ET and ER. Based on the clear delineation of the two growing seasons as shown by the GEP climatology, we examined the contribution and controls on the IAV of ecosystem carbon exchange in two growing seasons with an equal number of months: the “spring” growing season from January-June and the “summer” growing season from July - December. While there were a few years when the spring GEP continued into June or summer precipitation occurred during the last weeks of June, results were insensitive to whether June was included in the spring or summer total seasons because of the small amounts of carbon exchange and precipitation in June relative to the peak growing season months. Overall, we characterized a lower magnitude, but highly variable, spring period, and a higher magnitude,

but slightly less variable (relative to the means), summer period of physiological activity in this ecosystem.

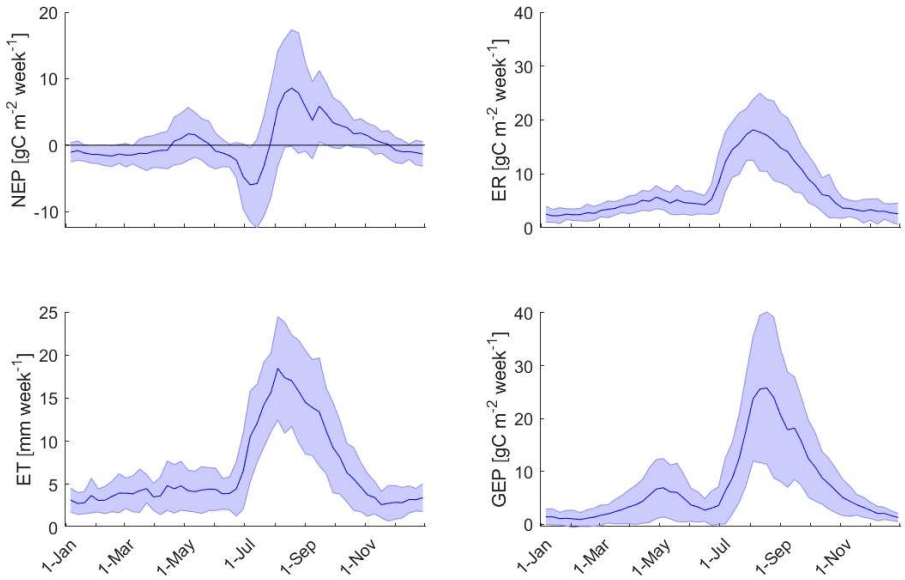

Figure 3. 2004-2022 weekly mean +/- 1 standard deviation of net ecosystem production (NEP), ecosystem respiration (ER), evapotranspiration (ET), and gross ecosystem productivity (GEP).

Our expected results are born out of shorter-term studies at this site or in this region. For the first objective, any hydrometeorological forcing or flux that can quantify water availability (precipitation, soil moisture, and evapotranspiration) should be closely related to gross ecosystem productivity (GEP) and ecosystem respiration (ER) (Biederman et al., 2016). Because of the close coupling of GEP and ER, net ecosystem production (NEP) should also be tightly linked to water and driven by changes in GEP (Biederman et al., 2017, 2016). In addition, we hypothesized that NEP would be more sensitive to water during the spring growing season than during the summer, based on results in other shrublands across the southwestern US showing higher springtime ratios of GEP/ER for a given amount of water (Biederman et al., 2018; Pérez-Ruiz et al., 2022; Petrie et al., 2015). For the second objective, we anticipated that the high interannual variability of precipitation drives equally high or even higher variability in carbon fluxes, which will make it difficult to identify significant C flux trends (Baldocchi et al., 2018). Still, because the site lies within the region experiencing among the most severe "megadrought" conditions since at least 800 CE (Williams et al., 2022), we expected that the associated high temperatures, vapor pressure deficit, and precipitation deficits (especially in the winter) may have

caused structural vegetation changes (e.g., declining cover and leaf area index [LAI], death of plants) that leads to persistent ecosystem carbon loss (Roby et al., 2020; Schwalm et al., 2012; Scott et al., 2015). For the third objective, we anticipated that satellite-based models will underestimate the variability of carbon and water fluxes but that newer products that incorporate an improved representation of moisture stress will better capture the IAV. Likewise, a calibrated land surface model (LSM) should predict carbon and water flux IAV better than a model that uses standard parameter sets as in global simulations (MacBean et al., 2021; Mahmud et al., 2021).

3. **Methodology**

Ecosystem Flux and Meteorological Measurements

The eddy covariance technique was used to measure ecosystem-scale CO_2, water vapor, and energy fluxes. Instrumentation on a 7 m tall scaffolding tower measured all variables needed to quantify 30-min averages of NEP, ET, air temperature (Ta), vapor pressure deficit (VPD), air pressure, photosynthetically active radiation (PAR), incoming and outgoing shortwave and longwave radiation, and precipitation (P). NEP is an ecosystem-centered metric of net CO_2 exchange; a positive value represents a net uptake and a negative value indicates a net release of CO_2 by the ecosystem. A specific instrumental bias in the sensitivity of each open-path infrared gas analyzer used at the site (IRGA, LI-7500, Li-Cor Inc) was discovered using side-by-side tests with other open-path and closed-path IRGAs. To correct for this bias and to ensure comparability across periods when different analyzers were deployed, we multiplied the 30-minute vertical wind and CO_2 density covariance by a bias correction factor determined individually for each IRGA through comparison with a closed-path analyzer (for more information see Scott et al., 2015)

The prevalence of data gaps in the meteorological data was low, usually less than 1% of all the 30-minute periods in each year. Except for P and PAR, these data were not gap-filled to compute annual and seasonal averages. The site has redundant precipitation gauges on separate dataloggers and another rain gauge is less than 1 km away. Differences in annual totals between the paired gauges were less than ~10 mm or 3%. In the case of failed primary gauge measurements, data from the other site gauge was used so that precipitation sums were gap-free. Missing PAR data, essential to partitioning and gap-filling fluxes, were either filled with a relationship using site-measured incoming solar radiation or PAR data from a nearby site (AmeriFlux site US-SRG, 5 km away).

The flux data were filtered for spikes, instrument malfunctions, and poor quality (representing ~7 – 11% of the ET and NEP data). The rejection criteria used to filter data included rain events, out-of-range signals, and spikes with variability of CO_2, water vapor , and/or sonic temperature greater than 2 standard deviations from the yearly mean. Daily ET was calculated by filling the gaps in the 30-minute data using 14-day moving-average look-up tables of ET and incoming PAR, averaged over 100-µmol m^{-2} s^{-1} intervals (Falge et al., 2001) and separated into morning (before 12 pm) and afternoon periods.

We partitioned NEP into gross ecosystem production (GEP) and ecosystem respiration (ER) by first eliminating NEP data when the friction velocity, u*, was less than 0.15 m s^{-1}. We then fit an exponential function of air temperature to the remaining nighttime NEP data over a moving ~5 day window (Reichstein et al., 2005) with varying window sizes to ensure that data from pre-storm (dry) periods were not grouped together with post-storm data; this step was necessary because precipitation events have been shown to result in immediate respiration pulses that change the relationship between temperature and nighttime NEP, equivalent to ER (Roby et al., 2020). The resultant exponential functions were used to fill missing nighttime NEP data and to model daytime ER. Missing daytime NEP values were filled using a second-order polynomial of incoming PAR, fit to separately to morning and afternoon data in a 5-day moving window. Finally, we calculated GEP as GEP = ER + NEP where GEP and ER are always greater than or equal to zero.

To examine the trade-off between carbon uptake and water loss, we calculated water use efficiency in a variety of ways (Knauer et al., 2017). At the ecosystem scale, the amount of gross productivity per unit of total water evaporated was defined as WUE_e = GEP/ET (gC $kg^{-1}H_2O$) for the summer growing season (Jul-Dec), for the peak growing months (Aug-Sep), and for peak August days when light and soil water were non-limiting (daily average PAR > 250 µmol m^{-2} s^{-1} and $VWC_{0\text{-}30cm}$ > 0.06 cm^3 cm^{-3}), focusing on the summer when most of the plants were actively photosynthesizing. Non-limiting light and soil thresholds were determined by plotting GEP:VWC or GEP:PAR and visually identifying where the relationships plateaued. For a more plant-centric metric that accounts for VPD limitations on stomatal conductance, we also quantified the underlying WUE, WUE_u = GEP* $VPD^{1/2}$/ET (S. Zhou et al., 2015). We averaged 30-min values of WUE_u under non-limiting light and soil water conditions (PAR > 800 µmol m^{-2} s^{-1} and $VWC_{0\text{-}30cm}$ > 0.06 cm^3 cm^{-3}), and only when evaporative losses were small (at least two days after rain). Results were comparable when including only data three or four days after rain.

Root-zone Volumetric Soil Water Content

Root-zone volumetric soil water content (VWC, cm^3-water cm^{-3}-soil) was measured with time-domain measurement probes (CS616, Campbell Scientific) installed at 2.5-5, 5-10, 15-20, 25-30, 45-50, 65-70, 95-100, and 125-130 cm depths. One inter-canopy profile was located ~10 m to the east of the flux tower below bunchgrasses and bare soil, and another under-tree profile was located under a nearby large (~5 m diameter crown) mesquite tree canopy about one-half the distance between the tree bole and crown edge. The under-tree profile lacked a probe at the 125-130 cm depth. We converted probe output to VWC using a second-order polynomial that was developed in the laboratory using soil from the site. Total 0-30 cm and 0-130 cm soil VWC for the two locations was determined by multiplying VWC at each depth by the thickness of each soil layer (7.5, 7.5, 7.5, and 7.5 cm or 7.5, 10, 15, 20, 25, 30, and 15 cm from shallow to deep, respectively), summing, and then dividing by the total depths. For the under-tree profile, we assumed that soil VWC at the 125-130 cm depth was equal to the 95-100 cm depth. We estimated site-average VWC using a weighted average of the profiles based on the tree-canopy fraction (0.30). While some studies have suggested that soil water potential may be a better metric to quantify ecosystem/plant available water (e.g., Novick et al., 2022), it is not commonly available and was not measured at this site, and VWC is commonly used to explain water and carbon flux variation (e.g., Kurc and Small, 2007; Vivoni et al., 2008).

Remote Sensing Flux Products

We evaluated site measurements of carbon and water fluxes against one vegetation index and seven satellite-based models that apply various approaches to estimate ET and GEP using radiance/reflectance data. Brief summaries of their spatial and temporal scales, along with the model approach and inputs are included below. We note that model products of GEP are often called gross primary production (GPP), which is equivalent to GEP.

1. MODIS Enhanced Vegetation Index (EVI, MOD13Q1; Huete et al., 2002): 0.25 km spatial resolution, 16-day temporal resolution, operational 2000-present. EVI is derived from atmospherically-corrected surface reflectance in the red, near-infrared, and blue wavebands. EVI minimizes canopy-soil variations and improves sensitivity over dense vegetation conditions relative to the normalized difference vegetation index (NDVI). Downloaded as 8.25 x 8.25 km subset centered on the tower (ORNL DAAC, 2018 https://doi.org/10.3334/ORNLDAAC/1567). A 3 x 3 pixel-area was averaged around the pixel containing the site.

2. MODIS ET (MOD16A2GF; Mu et al. 2011): 0.5 km spatial resolution, 8-day temporal resolution, operational 2000-present. Based on the Penman-Monteith model, where potential evapotranspiration is reduced under temperature and moisture stress. Remotely-sensed (RS) inputs are land cover, LAI, albedo, and the fraction of incident PAR absorbed by the canopy (FPAR); meteorological inputs are solar radiation, air pressure, Ta, and humidity (from GMAO reanalysis data).
3. MODIS GEP (MOD17A2GF; Running et al., 2004): 0.5 km spatial resolution, 8-day temporal resolution, operational 2000-present. Based on a light-use efficiency (LUE) model with "environmental stress" scalars that reduce photosynthesis below a biome-specific minimum temperature threshold and above a VPD threshold. RS inputs are FPAR and land cover; meteorological inputs are PAR, VPD, and Ta (GMAO).
4. SMAP GEP (SMAP L4C; Jones et al., 2017): 9 km spatial resolution, daily temporal resolution, operational 2015-present. GEP is simulated using a LUE model with "environmental stress" scalars that reduce photosynthesis below a biome-specific minimum temperature threshold, below a soil moisture threshold, above a VPD threshold, and when the ground is frozen. RS inputs are land cover, FPAR, surface and rootzone soil moisture, freeze/thaw status, and surface temperature; meteorological inputs are solar radiation, minimum Ta, and VPD (GEOS-5 Forward Processing system).
5. GLEAM ET (Martens et al., 2017; Miralles et al., 2011): 0.25^{o} (~30 km) spatial resolution, daily temporal resolution, available 2003-2021. ET is modeled as a function of potential evaporation (Priestley-Taylor), rainfall interception (Gash analytical model) and a cover-dependent stress factor, which is a function of microwave VOD and root zone soil moisture (calculated via a multi-layer water balance algorithm).
6. GLASS ET (Liang et al., 2021; Yao et al., 2014): 1 km spatial resolution, 8-day temporal resolution, available 2000-2018. A Bayesian fusion of five process-based or semiempirical algorithms: the MODIS ET algorithm (MOD16), the revised remote-sensing-based Penman-Monteith algorithm (RRS-PM), the Priestley-Taylor algorithm of the Jet Propulsion Lab (PT-JPL), a modified satellite-based Priestley-Taylor algorithm, and the Semiempirical Penman LE Algorithm of the University of Maryland.
7. GLASS GEP (Liang et al., 2021): 0.5 km spatial resolution, 8-day temporal resolution, available 2000-2020. Based on a revised Eddy Covariance-Light Use Efficiency (EC-LUE) model (Yuan et al., 2019), in which GEP is a function of direct and diffuse radiation, down-regulated based on Ta, VPD, and

atmospheric CO_2 concentration. Inputs are GIMMS3g NDVI (to estimate FPAR) and MERRA GMAO Ta, VPD, and PAR.

8. FluxSat v2.0 GEP (Joiner and Yoshida, 2020): 0.05° (~6 km) spatial resolution, daily temporal resolution, operational 2000-2020. GEP is upscaled by training a neural network to predict FLUXNET2015 GEP based on MODIS 7-band surface reflectance [MCD43C4] and top-of-atmosphere PAR, estimated as a function of the solar zenith angle.

The spatial resolutions of the satellite model estimates (0.25 - 9 km except for GLEAM ET, which is ~30 km) differ substantially from the footprint of the flux measurements, which have an average source area extending to approximately 200 m from the tower (and a range of ~100 - 1000 m, depending on atmospheric and surface conditions; Chu et al., 2021; Schmid, 1997). However, both spatial and temporal factors increase the comparability of the measurements and model estimates. The mesquite savanna around the flux tower extends for several kilometers in all directions around the site. While those distances span changes in soils, tree/grass percentages, stand age, and meteorology – most notably summer precipitation associated with spatially-discrete convective thunderstorm cells – we expect that the influence of forcing variability is considerably reduced when aggregating flux data seasonally (Goodrich et al., 2008). Also, satellite spectral indices (e.g., EVI) should integrate how precipitation, stand characteristics, and soils might affect vegetation productivity, effectively de-emphasizing the relevance of any single driver. A previous remote sensing study, based on this site and others in the lower elevation monsoon region, compared relationships of flux tower GEP with EVI and the Photochemical Reflectance Index (PRI) averaged over 3 km and 0.5 degree spatial scales, and found nearly identical temporal correlations at fine and coarse scales (Smith et al., 2018). Similarly, we found that the 16-day EVI data used in this study (3 x 3 0.25-km pixels centered on the tower pixel) was highly correlated with the average of the entire 8 x 8 km subset ($R^2 = 0.95$). Thus, satellite estimates derived from products at scales less than ~10 km (i.e., all except GLEAM) should capture the variability in the site conditions as sampled by eddy covariance.

Land Surface Model (LSM)

Carbon and water fluxes in LSMs are derived from process-based equations (e.g., leaf phenology, photosynthesis, respiration, stomatal conductance, and vertical soil moisture diffusion; Blyth et al., 2021) with fixed values (parameters) dependent on broadly defined plant functional types (PFTs) or soil texture. In this study, LSM estimates came from the ORCHIDEE v2.2 terrestrial biosphere model

(ORganizing Carbon and Hydrology In Dynamic EcosystEms; Dufresne et al., 2013; Krinner et al., 2005), which forms the land component of the French Institute Pierre Simon Laplace (IPSL) Earth system model. While there are many LSMs, MacBean et al. (2021) showed that all LSMs in the TRENDY v7 model intercomparison fail to capture variability in annual gross and net carbon fluxes. Across 12 sites in the Southwestern US, LSM gross and net CO_2 flux IAV and mean annual net carbon uptake were considerably underestimated by all TRENDY models. Teckentrup et al. (2021) reported similar results in TRENDY v8 across Australian FLUXNET sites, and Fawcett et al. (2022) demonstrated that TRENDY models have considerable biases in GPP and aboveground biomass across dryland regions globally. Here, we compared eddy covariance ET and GEP with site-scale ORCHIDEE simulations in land only mode, forced with site-measured meteorology, PFT fractional cover, and soil texture class. We applied ORCHIDEE with and without optimizing carbon and water cycle related parameters; parameters of the optimized version were calibrated against measured ET (Mahmud et al., 2023). Model outputs for both simulations (default and calibrated parameters) were available only from 2004 – 2012 due to an earlier termination of the modeling studies.

4. Results

Precipitation and Carbon Fluxes

For the 2004 - 2022 study period (Fig. 4), mean annual precipitation (P) was 360 +/- 103 mm (standard deviation) with 82 +/- 43 mm in the spring (January - July) and 277 +/- 85 mm in the summer growing season (July - December). In general, the first half of the US-SRM data record experienced drier springs and summers than the latter half. The study period overlaps the 21st-century “megadrought” across the western U.S. (Williams et al., 2022), which was indeed drier than the previous 30-yr (1974-2003) mean precipitation of 112 mm (spring), 295 mm (summer), and 407 mm (annual). However, the longer precipitation record for the Santa Rita Experimental Range from 1937-2003 reveals spring, summer, and annual averages (97 mm, 280 mm, 377 mm, respectively) only slightly higher than the current study period. The driest growing seasons during the current study were the spring of 2006 and the summer of 2020, and the wettest seasons were the spring and summer of 2018 (Fig. S1).

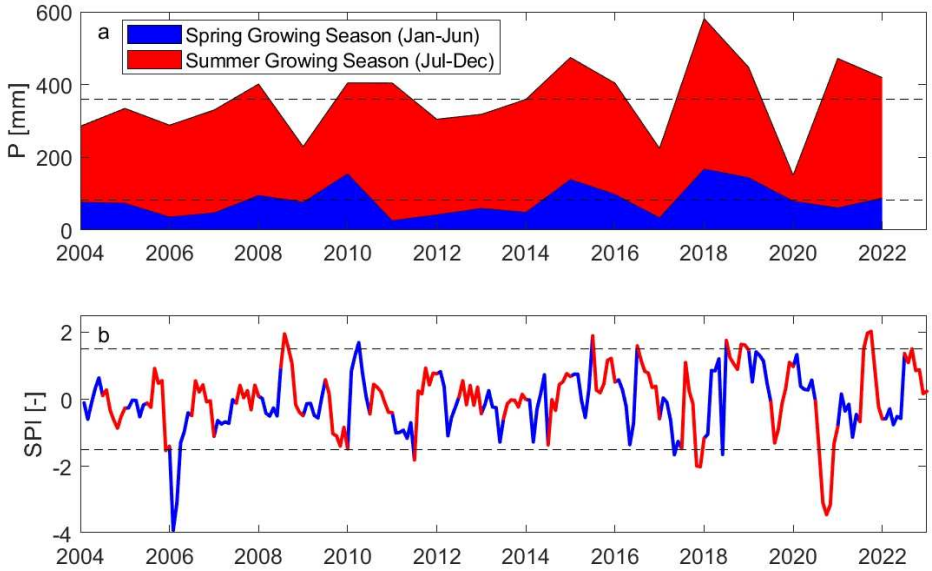

Figure 4. a) Annual precipitation (P) partitioned into spring and summer growing seasons with 2004-2022 average spring and annual totals indicated with dashed lines. b) Monthly Standardized Precipitation Index (SPI, 3-month) with dashed lines at -1.5 and 1.5 to indicate drought or pluvial conditions, respectively.

The interannual variability in precipitation at this savanna ecosystem translates to high variability in both gross and net carbon fluxes (Fig. 5). The ecosystem was a net sink for atmospheric CO_2 in twelve of the nineteen years, with the driest years generally resulting in negative NEP. Annually, NEP averaged 23 +/- 64 gC m^{-2}. Annual NEP was lowest in 2017, which had both a dry spring and summer, and highest in 2016 (wet spring and average summer, Fig. S1). Mean annual GEP was 372 +/- 122 gC m^{-2} and mean annual ER was 349 +/- 73 gC m^{-2}. Seasonally, spring periods were characterized by lower gross fluxes (GEP = 82 +/- 60, ER = 104 +/- 28 gC m^{-2}) and typically negative NEP (-22 +/- 37 gC m^{-2}) in contrast to higher gross fluxes (GEP = 290 +/- 117, ER = 245 +/- 68) and positive NEP for summer periods (45 +/- 58 gC m^{-2}). Annual GEP was more variable than ER with coefficients of variation equal to 33% and 21%, respectively, and was even more variable than P (CV = 29%). The only seasonal gross flux that was significantly correlated with annual NEP was summer GEP (R^2 = 0.49, $p < 0.01$).

392

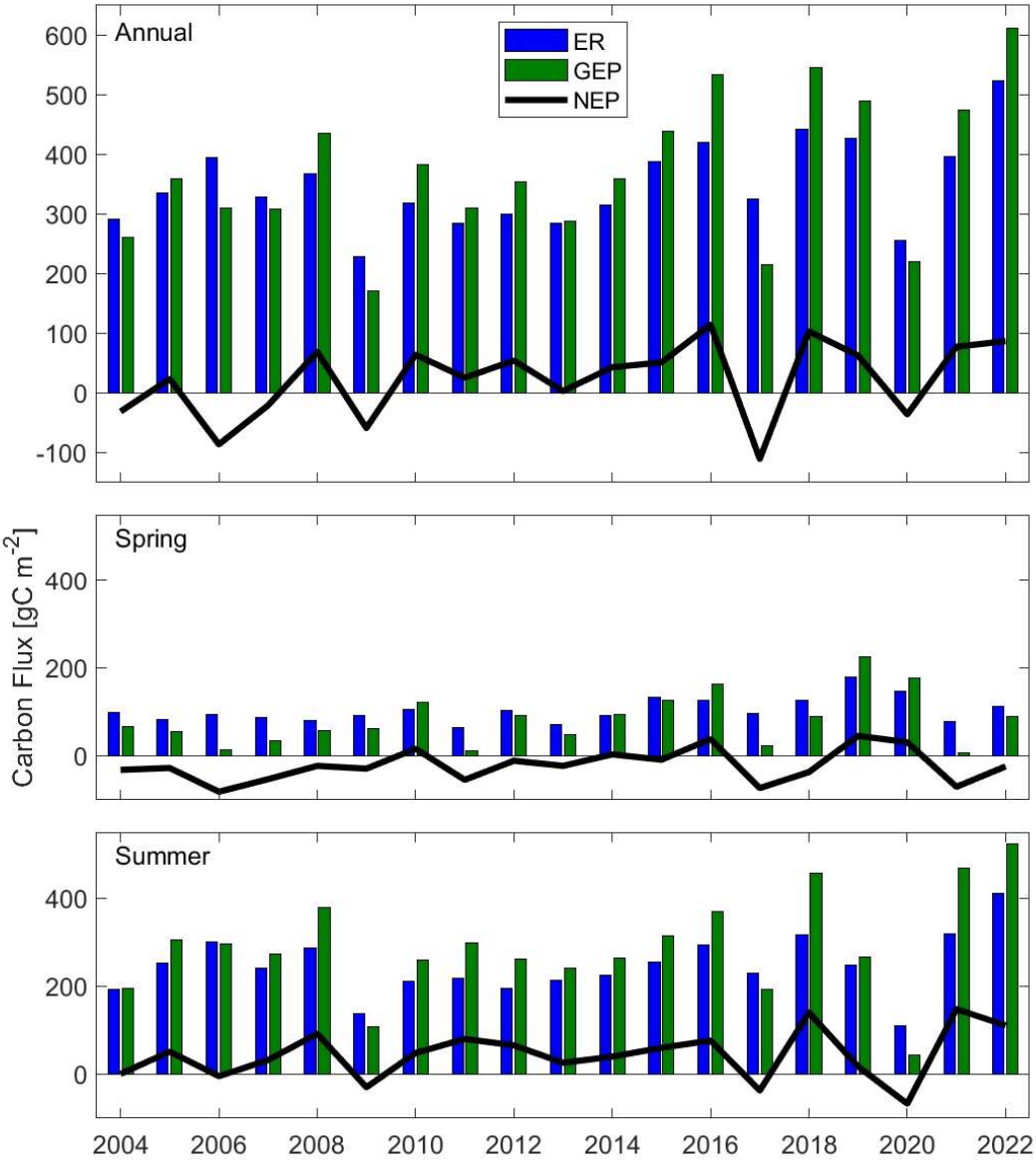

393

394 Figure 5. Annual, spring (Jan-Jun), and summer (Jul-Dec) growing season ecosystem respiration (ER,
395 blue), gross ecosystem productivity (GEP, green), and net ecosystem production (NEP, black).

396 Variation in summer and annual NEP was explained largely by precipitation (summer R^2 = 0.82, annual R^2
397 = 0.65; Fig. 6, Table 1). However, variability in spring NEP was poorly explained by spring P (R^2 = 0.29)
398 due to previously unutilized fall (October – December) precipitation stored as soil moisture that
399 contributes to spring productivity (Scott and Biederman, 2019). Thus, spring NEP was more correlated

with precipitation when October – December rainfall was included in the regression (R^2 = 0.80). Recognizing the effects of non-negligible storage between years, we defined a hydrological or *water year* with a start and end that occurs when storage is minimal, which at this site occurs most reliably in June (Fig. 2). Redefining annual P and NEP in water years improved their annual relationship (R^2 = 0.78, Fig. 6).

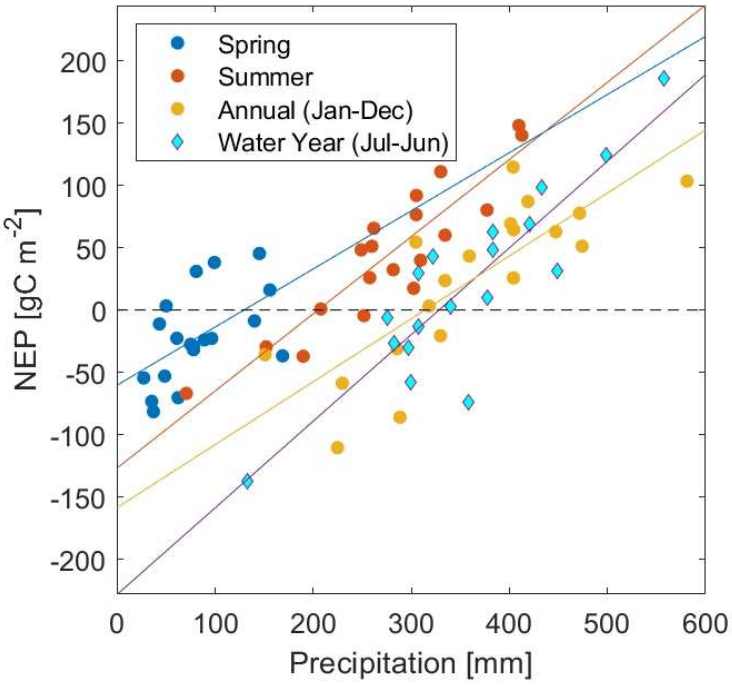

Figure 6. Spring (Jan-Jun), summer (Jul-Dec), annual (Jan-Dec) and water year (Jul-Jun) sums of precipitation and net ecosystem production (NEP).

In addition to precipitation, much of the variance in seasonal and annual NEP could also be explained by soil moisture (0-130 cm, though fits were only slightly worse for 0-30 cm) and greenness (Table 1). Annual P, soil VWC, and EVI typically explained less variance in NEP than seasonal values because spring and summer slopes and/or offsets were often season specific. We therefore explored the drivers of GEP and ER at the seasonal scale. To simplify presentation, we show results using VWC as the water availability metric because of its direct physical ties to plant photosynthesis and plant/soil respiration.

Table 1. Linear regression coefficients with slope (m), offset (b), and coefficients of determination (R^2) for spring, summer, and annual NEP predicted by P, VWC, and EVI.

NEP predicted by		m	b	R^2
P	spring	0.47	-60.16	0.29
	summer	0.62	-126.64	0.82
	annual	0.50	-158.33	0.65
VWC 0-130 cm	spring	2481.01	-185.13	0.70
	summer	5669.81	-332.37	0.69
	annual	6016.01	-375.15	0.51
EVI	spring	10.61	-266.68	0.58
	summer	10.26	-303.01	0.71
	annual	8.40	-456.92	0.47

Drivers of Seasonal Productivity and Respiration

Soil moisture explained much of the variation in both spring (R^2 = 0.85) and summer (R^2 = 0.73) GEP and ER (R^2 = 0.73 and 0.58, respectively, Fig. 7) and typically explained more of the variation than P (not shown). Slopes were greater for GEP than ER, indicating that soil moisture control on seasonal NEP was primarily driven by its effects on GEP. However, regression slopes were lower in spring than summer, implying that ecosystem metabolism was less sensitive to the same soil water status in spring than in summer. This was not due to averaging of elevated spring VWC values across the mainly dormant parts of spring (Jan-Feb, Figs. 2&3); the slopes of VWC regressions from March – June were similar to slopes of regressions from the entire January – June period (not shown).

Considering unexplained (by VWC) seasonal GEP variance (Fig. 7), GEP residuals were not significantly correlated with VPD or Ta in spring, but were correlated with VPD in summer (R^2 = 0.17, p = 0.08). Ta was correlated with ER residuals in spring (R^2 = 0.31, p = 0.01) but not with VPD or Ta in summer. Annual predictive power increased for both GEP (R^2 from 0.55 to 0.74) and ER (R^2 from 0.37 to 0.59) when separate seasonal regressions with VWC were used instead of annual values (Fig. 7).

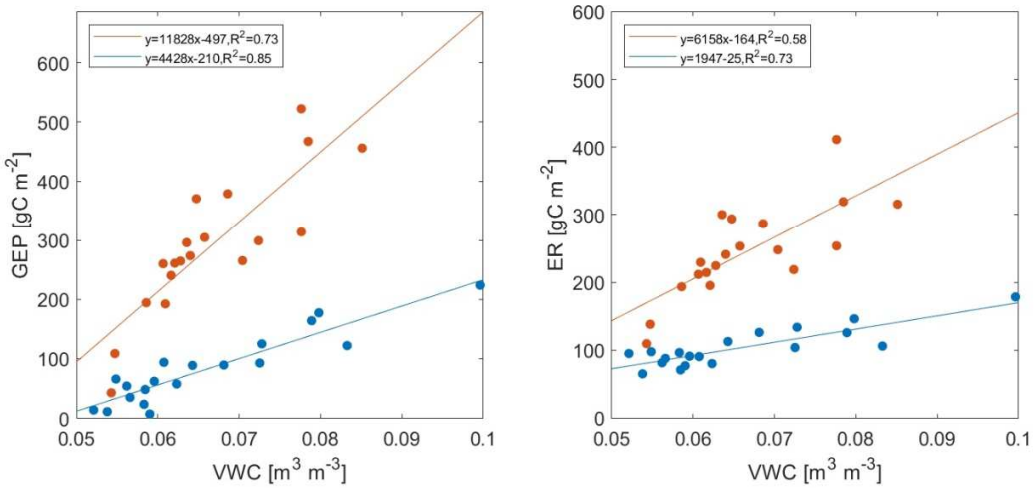

433
434 Figure 7. The relationship between soil volumetric water content (VWC, 0-1.3 m) and gross ecosystem
435 productivity (GEP) or ecosystem respiration (ER). Spring values are shown in blue, summer in red.

436

437 *Temporal Trends*

438 Longer flux tower records allow for the detection of trends in water and carbon fluxes. We used the
439 non-parametric Mann-Kendall τ (ranging from −1 to 1) to determine the degree to which trends were
440 present in the data, where τ = 1 indicates a monotonically increasing trend and τ = -1 indicates a
441 monotonically decreasing trend. Over the period of record (2004-2022), there were positive trends in
442 spring ER and annual NEP, GEP, and ER, but no significant changes ($p > 0.10$) in ET (Table 2). Over the
443 same period, concentrations of atmospheric CO_2 increased 2.58 ppm/yr, 49 ppm, or about 13% (data not
444 shown), which may partly explain increases in GEP and NEP without an associated increase in ET due to
445 increased plant water use efficiency (Walker et al., 2021). However, annual P, VWC (both depths), and
446 EVI also increased (Table 2), as did spring and summer VWC for 0-0.3 m depth and spring EVI.
447

Table 2. 2004 – 2022 trend results for the spring, summer and annual site meteorology and fluxes. Numbers indicate Mann-Kendall τ values, with bold values denoting

statistically significant increases (+ τ) at p < 0.10(*) and p < 0.05(**).			
	Spring	Summer	Year
P	0.18	0.26	**0.29***
Ta	**0.29***	0.10	0.25
VPD	0.24	0.11	0.05
VWC 0-1.3m	**0.42****	0.25	**0.45****
VWC 0-0.3m	**0.45***	**0.36****	**0.52****
EVI	**0.31***	0.25	**0.35****
NEP	0.23	0.17	**0.32***
GEP	0.25	0.19	**0.35****
ER	**0.31***	0.27	**0.29***
ET	0.15	0.12	0.18

Focusing in on the summer growing season when there is maximum plant photosynthesis, ecosystem water use efficiency (WUE_e) and underlying water use efficiency (WUE_u) computed over various times and conditions were highly variable (Fig. 8), with decreases in dry years and increases in wet years. There were no significant trends in either metric at any time or condition analyzed, but there were clear increases in the summers of 2021 and 2022 as the ecosystem was released from the severe drought that lasted from the 2020 summer through the 2021 spring.

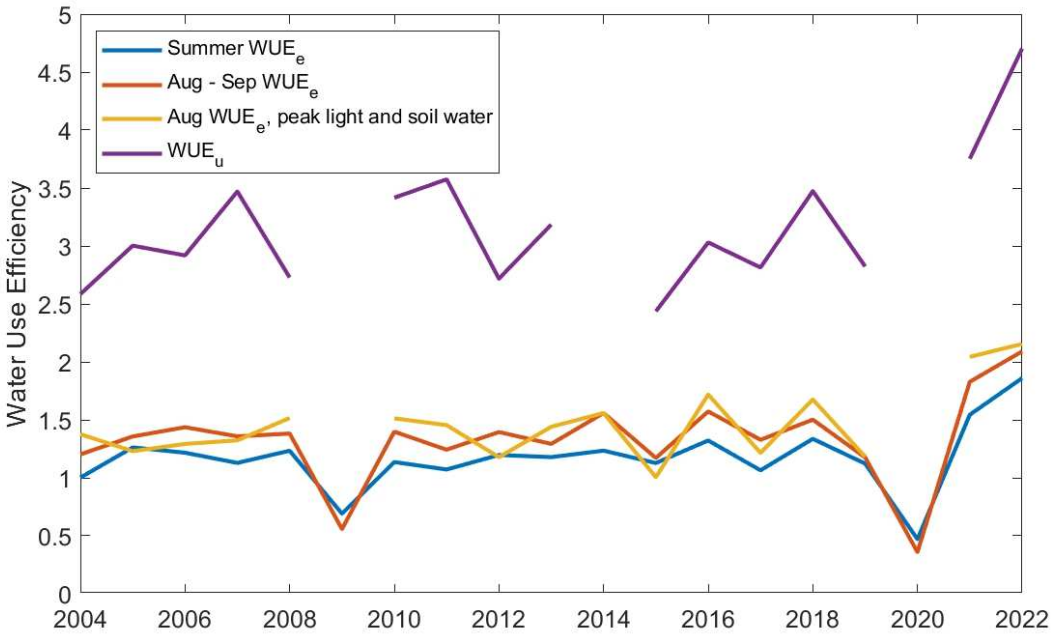

455

456 Figure 8. Mean daily ecosystem water use efficiency (WUE_e = GEP/ET) for the summer growing season,
457 the months of August – September, and peak, non-water limiting, and non-light limiting conditions in
458 August. Also shown is the mean underlying water use efficiency (WUE_u = GEP* $VPD^{1/2}$/ET) under optimal
459 (see Methods) growth conditions in August. Missing years indicate that there were no values with
460 optimal conditions.

461 *Satellite and Land Surface Models*

462 We examined whether state-of-the-art models can reproduce the seasonal and annual variability of the
463 measurements. Here, we focused on two key variables: GEP for the fundamental role it plays in the IAV
464 of NEP, and ET as a metric of site water availability that can also be estimated using satellite data and
465 associated models. While ET is a flux, rather than an ecosystem state variable, it has previously been
466 shown to be an excellent predictor (explaining more variance than P and VWC) of carbon fluxes at this
467 and other dryland sites (Biederman et al., 2016; Scott et al., 2015; Scott and Biederman, 2019).
468
469 Models of seasonal ET (0.5 km MODIS, 30 km GLEAM, 1 km GLASS, default and optimized ORCHIDEE)
470 differed substantially in their agreement with site measurements (Fig. 9). Satellite model regression
471 slopes ranged from 0.27 to 0.71 for spring and from 0.10 to 0.61 for summer. Biases in the seasonal
472 magnitudes were largest for MODIS, while GLASS had very little variability from year to year (slope =

0.27 for spring; 0.10 for summer). In spring, the ORCHIDEE LSM tended to underestimate ET at low values and overestimate at high values; in summer, ORCHIDEE slopes were 0.64 and 0.89 for default and optimized simulations, respectively.

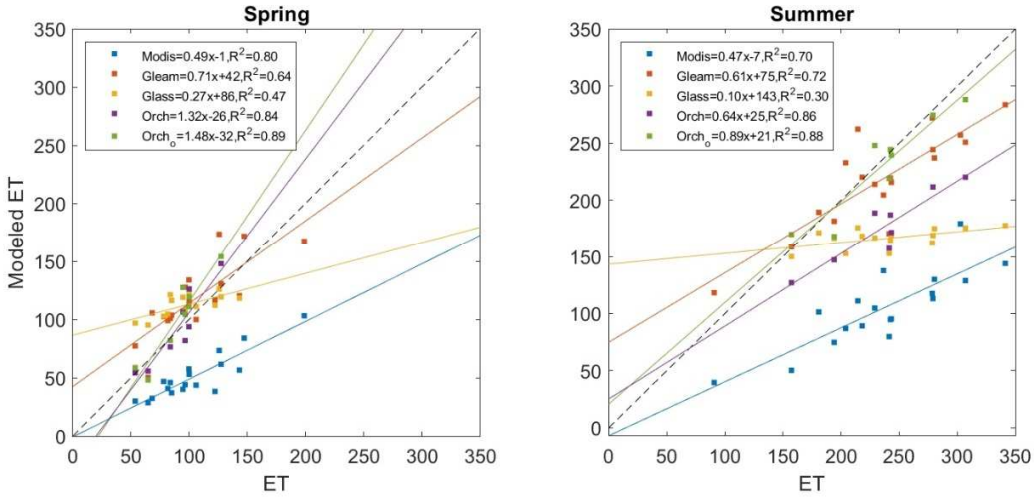

Figure 9. Measured and modeled spring and summer growing season evapotranspiration (ET, mm) totals. The 1:1 line is dashed and the colored lines represent best-fit regressions. ORCHIDEE simulation results are for default (Orch) and optimized ($Orch_o$) parameters.

The IAV of GEP was underestimated by all models, as demonstrated by measured vs. modeled GEP regression slopes substantially <1 for all models in both seasons (slopes ranged 0.31 – 0.55 in spring and 0.36 – 0.71 in summer; Fig. 10). In most cases, GEP was overestimated in spring (values above the dashed 1:1 line) and underestimated in summer (values below). This resulted in compensating errors when determining mean annual sums, but also indicated a failure to capture even the general bimodal seasonal pattern of GEP at this site (Fig. 3) with substantially lower values in spring and higher values in summer. Optimization of ORCHIDEE carbon and water cycle parameters using ET as a constraint improved the slope and underestimation of summer GEP but did not notably improve spring simulations.

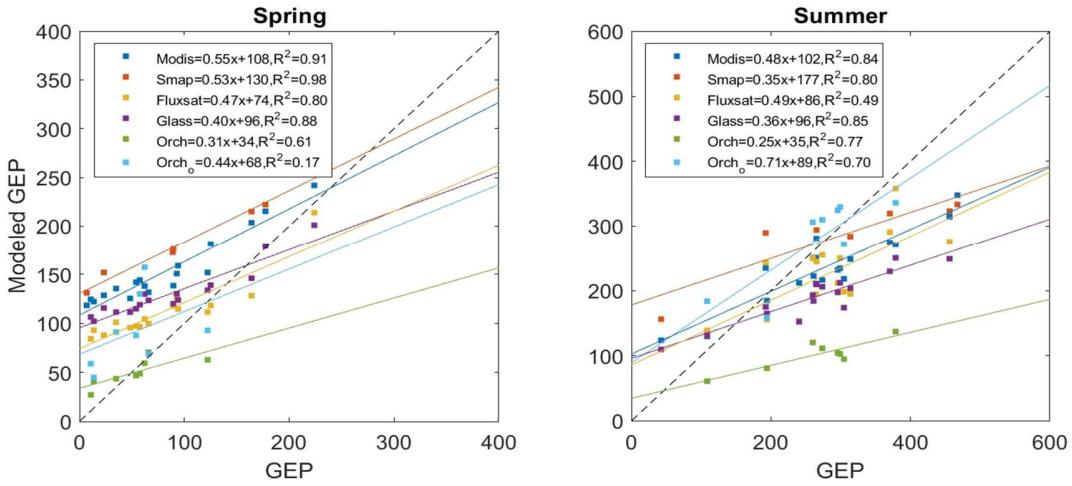

Figure 10. Measured vs. modeled spring and summer growing season gross ecosystem productivity (GEP, gC m^{-2}) totals. ORCHIDEE simulation results are for default (Orch) and optimized ($Orch_o$) parameters.

5. Discussion

Short-term ecosystem flux studies are useful for understanding the magnitudes and seasonality of the fluxes at a site, but their conclusions are constrained by the meteorological and ecosystem conditions during the study period. As site records lengthen, it is possible to resolve flux means, variability, and trends, as well as environmental drivers of those flux quantities, with higher confidence (Figs. 2 and 3). As we celebrate the 25th anniversary of AmeriFlux, data records for sites are beginning to span one and even two decades. Here, we were able to constrain longer-term processes using 19 years of micrometeorological measurements at a semiarid savanna site.

Long-term monitoring is essential to capture dryland ecosystem response to interannual climatic variability and decadal climate shifts like long-term drought. In general, the first half of the US-SRM record experienced drier springs and summers than the latter half, corresponding to the "turn-of-the-21st century" drought, which was associated with large reductions in carbon uptake throughout the western U.S. (Cayan et al., 2010; Schwalm et al., 2012). As drought conditions continued into the 2010's, the 21st-century "megadrought" emerged across the southwestern U.S. (Williams et al., 2022), and site conditions were indeed drier than the previous 30-year means. However, they were only slightly drier than the longer-term precipitation record at the site. This result highlights that defining the period for

509 determining average or baseline climatic conditions, as well as ecosystem responses, may affect what is
510 seen as normal versus anomalous in a changing climate (Milly et al., 2008).

511 One of the ways that megadrought status is assessed is by using cumulative 0-2 m soil moisture
512 anomalies from a bucket-type water balance model forced with climate data, where anomalies are
513 defined as differences from long-term climatological soil moisture values (Williams et al., 2022). This
514 may be a good metric to describe cumulative drought stress for human systems like agriculture and
515 water supply that have large amounts of water storage (e.g., groundwater basins, man-made
516 reservoirs), but it is not appropriate for quantifying the water status of dryland ecosystems that may
517 experience some seasonal storage/carryover of water (e.g., spring moisture adding to summer growth,
518 or late fall/ winter moisture for spring growth) but not from year to year. For example, every June at US-
519 SRM, the soil moisture storage was drawn down so there would be little or no hydrological memory of
520 previous year's precipitation. Still, ecosystem carbon cycle legacies can result from shifts in precipitation
521 (decadal-scale droughts and pluvials) as carbon stocks (e.g., aboveground/belowground biomass, soil
522 carbon) adjust over longer timescales. Carbon cycling trajectories following disturbance are well-studied
523 in forested ecosystems using chronosequences (Fu et al., 2017), but much less is known about them in
524 dryland ecosystems, though some results suggest that adjustments may be more rapid (years, rather
525 than decades; Ma et al., 2016; Scott et al., 2015).

526 Below, we discuss whether our results support our specific hypotheses:

527 *1) Investigate coupling between the interannual variability of hydrometeorological drivers and*
528 *ecosystem carbon fluxes*

529 As expected, water availability was the dominant driver of carbon cycling in this savanna. The ecosystem
530 carbon fluxes at US-SRM rapidly responded to variations in precipitation (CV = 29%), with plants quickly
531 adding leaf area and accumulating biomass in years of abundance and quickly decreasing carbon uptake
532 in dry years (Figs. 4 and 5). As expected for dryland regions, the large interannual variability of P and
533 associated root zone soil moisture led to a large variability in NEP (mean = 23 +/- 64 gC m^{-2} yr^{-1}, Fig. 6,
534 Table 1). Other long-term flux studies at mesic forested sites have shown similar variability (standard
535 deviation = ~50 – 100 gC m^{-2} yr^{-1}), but with considerably higher means (~100 – 500 gC m^{-2} yr^{-1}; Beringer
536 et al., 2022; Desai et al., 2022; Finzi et al., 2020). Throughout the lower elevation sites in the
537 southwestern U.S. and northwestern Mexico region, Biederman et al. (2017) found that about half of
538 the 25 flux sites analyzed pivoted between annual net carbon loss during dry years and carbon gain

539 during wet years, especially in the lower monsoon region (Fig. 6; Scott et al., 2015). The NEP of dryland
540 sites on other continents (e.g., Australia and Spain) similarly pivoted depending on P, showing that
541 carbon exchanges are resilient to the frequent drought and pluvial cycles experienced in these regions
542 (El-Madany et al., 2020; Tarin et al., 2020). While a strong relationship between total summer P and NEP
543 may be surprising given the well-known precipitation pulse-driven responses characteristic of
544 thunderstorm-driven drylands (Huxman et al., 2004), we note that summer P totals were closely related
545 to the amount of rainfall occurring in the larger, more biologically-significant pulse events (P > 10 mm
546 day^{-1}, Fig. S2), which stimulate and sustain GEP increases to a greater degree than ER (Roby et al., 2022).
547 Thus, summer P totals reflected the number and amount of these less frequent but disproportionately
548 important pulse events.

549 Given that the variability of GEP (CV=33%) was higher than that of ER (CV=21%), NEP variations were
550 principally driven by GEP as hypothesized. The annual variability of NEP from dryland flux sites at other
551 sites in the southwestern U.S. is similarly explained by GEP variability (Biederman et al., 2017). Out of all
552 seasonal flux totals at US-SRM, only summer GEP was correlated with annual NEP, indicating that the
553 summer growing season was a key determinant of the annual carbon balance. In this savanna,
554 phenocam measures of separate tree and grass greenness responses indicate that summertime
555 greenness is dominated by the C4 grass understory rather than the C3 trees (Steiner, 2022). While
556 greenness from satellites and phenocams can be less coupled to productivity at hourly to weekly
557 timescales because of strong stomatal regulation in response to soil and atmospheric dryness, the
558 monthly-to-annual greenness tends to approximate GEP (Browning et al., 2017; Ma et al., 2013; Yan et
559 al., 2019). Studies of flux IAV across precipitation gradients have shown similarly variable GEP and ER at
560 other semiarid grassland and shrubland sites (Biederman et al. 2017) that decrease considerably at
561 wetter, forested sites (mean GEP CV = 0.13 and mean ER CV = 0.12, Baldocchi et al., 2018).
562
563 The savanna showed different carbon flux responses to variations in water availability during the spring
564 and summer growing seasons (Figs. 6 and 7). The precipitation pivot point (P = 96 mm where NEP = 0)
565 tended to be higher than the mean spring P (82 mm), such that only wetter-than-normal springs had net
566 carbon gains (Fig. 6), contrary to our hypothesis that spring NEP would be more responsive to P due to
567 decreased ER relative to GEP. The opposite was true for summer (pivot point = 217 mm P, average = 277
568 mm P), such that most summers were characterized by positive NEP. During both growing seasons, soil
569 moisture explained much of the variability in GEP and ER, but there was lower GEP and ER for a given
570 VWC in spring than in summer (Fig. 7). This may be associated with the reduced activity of the

understory C4 grasses in spring compared to summer (Cable, 1975; Kemp, 1983; Steiner, 2022). Conversely, the relatively higher influence of C3 trees on spring GEP is likely why spring productivity at the savanna was less water use efficient than summer (mean spring WUE_e = 0.70 vs. 1.17 for summer). This reduced WUE contrasts with C3-dominated shrubland sites in the region, which have a propensity for higher NEP in spring than summer due to consistent WUE and less ER relative to GEP in spring (Biederman et al., 2018; Pérez-Ruiz et al., 2022).

2) Quantify trends in hydrometeorological drivers and ecosystem carbon fluxes during the spring and summer growing seasons

Even with nearly two decades of data, we hypothesized that the high variability in water availability, the dominant driver of carbon flux IAV at this site, would make it difficult to identify trends over the 19-year record. However, we found statistically significant increases in Ta, VWC, and EVI in spring, VWC in summer, and in annual P, VWC and EVI (Table 2), which both influence and are influenced by water and carbon fluxes. Spring ER increased significantly during 2004-2022 in accord with increased temperatures and near-surface soil moisture. Soil moisture is a primary control of soil respiration in drylands, and has been shown to both explain substantial variability in efflux rates and regulate the temperature response of soil respiration at this site (Roby et al., 2022, 2019). Also, small positive, but non-significant, trends in spring and summer GEP, ER, and NEP contributed to significant increases in annual GEP, ER, and NEP over the study period. These trends were likely driven by changes in precipitation (regression line slope of 5.5 mm yr^{-1}) transmitted through soil moisture. Generally, the early years of monitoring were drier with lower fluxes, while the later years were wetter with higher fluxes (Fig. 4 and 5).Thus, we found little evidence that the southwestern US megadrought conditions continued into the later half of the monitoring period nor that it caused ecosystem structural changes (e.g., plant mortality and dieback resulting in less soil carbon inputs and plant matter decay) that could lead to persistent carbon loss from the savanna (Huang et al., 2018; Throop and Archer, 2007). Plant cover surveys suggest that such a structural adjustment for both woody and grass cover happened in the decade preceding the start of flux tower monitoring (Fig. S3) with large decreases in cover following the wet 1980's and early 1990's.

There was considerable variability in the trade-off between productivity and evapotranspiration (i.e., WUE) of the savanna, especially during the last three years. All WUE metrics were dramatically reduced during the record summer drought in 2020 (Fig. 4), but subsequently responded to abundant summer rains and increased to their highest levels in 2021 and 2022 (Fig. 8). It is likely that this dramatic rebound, or 'whiplash' (Swain et al., 2018), was driven by increasing LAI and GEP associated with

602 flourishing understory grasses and mesquite trees in 2021 and 2022 and captured by increasing EVI.
603 Nearby long-term vegetation transects showed a doubling in grass basal cover and a 10% increase in
604 tree/shrub canopy cover from measurements prior to the 2020 summer drought (Fig. S3). This
605 abundance led to noticeable decreases in bare soil cover that altered the amount of GEP relative to the
606 ET during this season (Figs. 8 and S4).

607 Applying the Scott and Biederman (2017) approach to estimate long-term abiotic evaporation (E) at US-
608 SRM prior to 2021, we found an average summer E/ET ratio of 0.32 (or, [transpiration, T]/ET = 0.68).
609 However, 2021 and (especially) 2022 did not conform to the close relationship between GEP and ET in
610 prior summers (Fig. S4); there was lower soil evaporative loss relative to ET during these years. Reasons
611 for this could include increased cover acting as a mulch (less E) and/or improved scavenging of soil
612 moisture due to more surface roots (more grass T). Furthermore, across dryland sites, increased water
613 availability leads to higher WUE_e, in part due to increased LAI that increases T/ET (Scott et al., 2015).
614 Thus, the trends in carbon fluxes at US-SRM are likely due to increasing plant water availability
615 supporting more leaf area, rather than changes in leaf-level water use efficiency associated with carbon
616 dioxide fertilization, as found for forested flux sites in the northeast U.S. (Keenan et al., 2013). We
617 expect that changes in leaf-level water use efficiency (i.e., carbon fertilization) might be harder to detect
618 in drylands at the ecosystem scale, even more so than they are in north-central U.S. forests (Desai et al.,
619 2022), because of drylands' greater proportion of abiotically-driven processes (E, heterotrophic ER) to
620 biotically-driven processes (T, autotrophic ER, GEP) in the composite fluxes (ET and NEP, Wang et al.,
621 2021).

622 *3) Assess the ability of modern land surface and satellite models to reproduce the IAV of carbon and*
623 *water fluxes*

624 Satellite and LSM estimates of ET, GEP, and NEP are routinely used to assess water and carbon cycle
625 trends and variability, as well as their responses to climatic change and extreme weather events. They
626 have also been used to identify key regions driving the response of the biosphere to anthropogenic
627 change, and they have identified drylands as hotspots for carbon sink variability (Ahlström et al., 2015;
628 Poulter et al., 2014). Satellite models are typically assessed globally with a large compilation of site data
629 from data products like FLUXNET2015 (Pastorello et al., 2020) and are thus shown to work across sites
630 (spatially) rather than through time (e.g., Jones et al., 2017; Liang et al., 2021; Running et al., 2004).
631 Correspondence between models and measurements at locations through time is comparatively less
632 well-studied.

While considerable effort has been expended to develop satellite-based estimates of ET, especially for agricultural and forestry applications (Anderson et al., 2011; Melton et al., 2022), dryland ET variability is often underestimated (Biederman et al., 2017; Dannenberg et al., 2023). Yet, dryland ET represents an integrated measure of ecosystem water availability, and explains a large part of dryland carbon flux variability (Biederman et al., 2016). Of the satellite models we examined, GLEAM (30 km resolution) more closely matched the range of tower-observed ET variability during both growing seasons (Fig. 9, slopes of 0.71 and 0.61) than MODIS (0.5 km, slopes of 0.49 and 0.47) or GLASS (1 km, slopes of 0.47 and 0.10). This was unexpected given GLEAM's coarse spatial resolution relative to the tower footprint, but it may highlight the importance of particular variables and processes – namely soil water availability and plant water use – for controlling dryland ET. Unlike MODIS and GLASS, GLEAM includes vegetation optical depth, which is directly related to plant water status and water use strategies (e.g., Konings and Gentine, 2017). It also includes estimates of soil moisture, which drive variability in dryland surface conductance (e.g., Novick et al., 2016). The severe underestimation of ET IAV by GLASS may be associated with the weighted-average approach (reduces variance compared to the individual model estimates that compose the ensemble) and its tuning based on the global FLUXNET network, which was dominated largely by temperate flux sites (Yao et al., 2014). MODIS ET also underestimated ET in both seasons, which may be associated with its lack of an explicit soil moisture control (Brust et al., 2021).

The ORCHIDEE model (local meteorology with default parameters) captured over 80% of variation in ET. Parameter optimization improved the slope of the summer regression line from 0.64 to 0.89 but did not improve the slope or bias for the spring (Fig. 9). Together, these results corroborate previous suggestions that diverse mechanisms for plant water uptake, transport, storage, and loss by multiple plant functional types (e.g., trees versus grasses) require more realistic representation in models (MacBean et al., 2021; Whitley et al., 2017). Dryland-specific plant photosynthetic and water use traits (e.g., Barron-Gafford et al., 2012) and improvement of phenology modules are also likely to improve model-data mismatches, and can be used to test the validity of calibrated parameters (Mahmud et al., 2021; Teckentrup et al., 2021).

As with ET, satellite models underestimated the IAV of GEP (Fig. 10), capturing only 40 to 53% of spring and summer variability. Moreover, the models did not reproduce US-SRM's bimodal growing season: nearly all the spring estimates were biased high, and many of the summer estimates were biased low. This result suggests that static model parameterizations were unable to accommodate structurally and functionally variable ecosystems. For example, the LUE models (SMAP, GLASS, and MODIS) include

664 biome-specific (but temporally unchanging) parameterizations for “optimal” LUE and
665 temperature/water stress scalar functions. For a pulse-driven semiarid savanna, where the fractional
666 covers of annual and perennial grasses vary seasonally and interannually depending on water status,
667 static LUE and scalar functions may not be sufficient (Chang et al., 2020). Further, only SMAP includes
668 soil moisture as a potential water stress down-regulator for optimal LUE, despite the fundamental
669 relevance of soil moisture, rather than VPD, in dryland ecosystem functioning (Novick et al. 2016).
670 Finally, it is notable that Wang et al. (2022) found significant seasonal biases in the ability of optical
671 reflectance—on which all the satellite-based models examined here are partly based—to track dryland
672 GEP. They report overestimation of GEP prior to the peak growing season and underestimation after,
673 which increased as woody plant cover increased.

674 The ORCHIDEE model did a much poorer job of simulating the IAV of GEP relative to ET; however,
675 optimizing for ET did result in improvements. As a result, more work is required to explore whether
676 parameter calibration is responsible for model structural errors (Mahmud et al., 2021). For example,
677 processes that are important for dryland carbon and water cycling, such as biological soil crust activity,
678 are omitted from this and other LSMs (Osborne et al., 2022).

679 Flux datasets spanning one to two decades afford new opportunities to assess the capability of satellite
680 models and LSMs to predict the interannual variability of land-atmosphere water and carbon fluxes.
681 Model testing focused on site-scale variability is a particularly promising avenue for model development
682 because site-scale comparisons are focused on the temporal patterns often obscured by cross-site
683 comparisons. While key uncertainties in measured fluxes include lack of energy balance closure and NEP
684 partitioning, we expect that these are more relevant to flux means than their variability (Baldocchi,
685 2008; Baldocchi et al., 2018; Lasslop et al., 2010). Thus, model testing focused on site variability may
686 effectively diagnose model formulation and parameterization errors, leading to improved confidence in
687 modeling study conclusions (Keenan and Williams, 2018).

688 **6. Conclusions**

689 The high IAV of both net and gross CO_2 fluxes was very closely related to water availability at the US-
690 SRM savanna, which was mainly dependent on recent precipitation, with little long-term storage to
691 buffer periods of water scarcity. Specifically, the NEP, GEP, and ER rapidly responded to interseasonal
692 and interannual variability in water availability with no identifiable hydrological memory. We also found
693 that climatic variability, even during this relatively short period, was significant with generally drier

conditions in the first half of the monitoring period and wetter conditions in the latter half. In addition, there were large whiplashes in the precipitation record; for example, from record summer and winter drought in 2020 to abundant rains in 2021 that may have induced ecosystem structural changes that altered WUE. With the easing of the turn-of-the-21st century drought, there were positive trends in annual P and seasonal and annual VWC, and the ecosystem responded with positive trends in CO_2 fluxes. While the longer flux record allowed for a more robust characterization of the flux IAV and its controls, the multi-scale episodic nature of water inputs to this savanna and other dryland regions make it difficult to identify a stable or stationary period on which to base firm conclusions about mean ecosystem flux behavior.

As AmeriFlux reaches its milestone 25th year, we celebrate that ecosystem flux research continues to add analytical facets that refine understanding of ecosystem function. In this case, we leveraged 19 years of continuous flux data to focus on a more robust quantification of IAV and decadal-scale variability as well as to identify trends due to both short-term disturbances and long-term climatic and structural change. In this way, continuous datasets are especially critical to understanding and predicting ecosystem dynamics at dryland sites where the variability of fluxes makes it difficult to quantify mean responses. Although modern satellite estimates and LSMs are essential tools for understanding IAV of the terrestrial carbon sink, these models performed poorly at US-SRM. As a result, the cuttent study highlights the advantage of using long-term datasets to resolve model-data disagreements, especially for the purpose of capturing seasonal to annual variability.

Acknowledgments

Data used in this paper are available at the AmeriFlux Data Repository (http://ameriflux.lbl.gov/) or upon request to the corresponding author. This work was supported by USDA-ARS, and funding for the US-SRM AmeriFlux Core Site was provided by the U.S. Department of Energy Berkeley National Labs. MPD and MRJ were supported by NASA grant 80NSSC20K1805. Long-term monthly precipitation and vegetation transect data were provided by the Santa Rita Experimental Range Digital Database (https://cals.arizona.edu/srer/content/data-resources), with funding provided by USDA Forest Service Rocky Mountain Research Station and the University of Arizona, Arizona Experiment Station. Remote sensing data can be obtained from: FLUXSAT (https://daac.ornl.gov/cgi-bin/dsviewer.pl?ds_id=1835), GLEAM (https://www.gleam.eu/#downloads), GLASS (http://www.glass.umd.edu/Download.html),

MODIS (https://appeears.earthdatacloud.nasa.gov/), and SMAP (https://nsidc.org/data/smap/data). The model outputs from ORCHIDEE simulations are stored in Figshare at https://doi.org/10.6084/m9.figshare.21944975.v1. We thank the ORCHIDEE Project and Data Assimilation Teams for developing and maintaining the ORCHIDEE code and for providing the ORCHIDEE version 2.2 and data assimilation systems used in this study. We also thank A. Gorlier (U. Arizona) and M. McClaran (U. Arizona) for collecting and helping to process Santa Rita Experimental Range vegetation cover data. USDA-ARS is an Equal Opportunity Employer.

7. **Bibliography**

Adams, D.K., Comrie, A.C., 1997. The North American Monsoon. Bull. Am. Meteorol. Soc. 78, 2197–2213.

Ahlström, A., Raupach, M.R., Schurgers, G., Smith, B., Arneth, A., Jung, M., Reichstein, M., Canadell, J.G., Friedlingstein, P., Jain, A.K., 2015. The dominant role of semi-arid ecosystems in the trend and variability of the land CO2 sink. Science 348, 895–899. https://doi.org/10.1126/science.aaa1668

Anderson, M.C., Kustas, W.P., Norman, J.M., Hain, C.R., Mecikalski, J.R., Schultz, L., Gonzalez-Dugo, M.P., Cammalleri, C., d'Urso, G., Pimstein, A., 2011. Mapping daily evapotranspiration at field to continental scales using geostationary and polar orbiting satellite imagery. Hydrol. Earth Syst. Sci. 15, 223–239. https://doi.org/10.5194/hess-15-223-2011

Anderson-Teixeira, K.J., Delong, J.P., Fox, A.M., Brese, D.A., Litvak, M.E., 2011. Differential responses of production and respiration to temperature and moisture drive the carbon balance across a climatic gradient in New Mexico. Glob. Change Biol. 17, 410–424. https://doi.org/10.1111/j.1365-2486.2010.02269.x

Baldocchi, D., 2008. Turner Review No. 15. "Breathing" of the terrestrial biosphere: Lessons learned from a global network of carbon dioxide flux measurement systems. Aust. J. Bot. 56, 1–26.

Baldocchi, D., Chu, H., Reichstein, M., 2018. Inter-annual variability of net and gross ecosystem carbon fluxes: A review. Agric. For. Meteorol. 249, 520–533. https://doi.org/10.1016/j.agrformet.2017.05.015

Baldocchi, D.D., 2003. Assessing the eddy covariance technique for evaluating carbon dioxide exchange rates of ecosystems: Past, present and future. Glob. Change Biol. 9, 479–492.

Baldocchi, D.D., Hicks, B.B., Meyers, T.P., 1988. Measuring biosphere-atmosphere exchanges of biologically related gases with micrometeorological methods. Ecology 69, 1331–1340.

Barba, J., Cueva, A., Bahn, M., Barron-Gafford, G.A., Bond-Lamberty, B., Hanson, P.J., Jaimes, A., Kulmala, L., Pumpanen, J., Scott, R.L., Wohlfahrt, G., Vargas, R., 2018. Comparing ecosystem and soil respiration: Review and key challenges of tower-based and soil measurements. Agric. For. Meteorol. 249, 434–443. https://doi.org/10.1016/j.agrformet.2017.10.028

Barron-Gafford, G.A., Sanchez-Cañete, E.P., Minor, R.L., Hendryx, S.M., Lee, E., Sutter, L.F., Tran, N., Parra, E., Colella, T., Murphy, P.C., Hamerlynck, E.P., Kumar, P., Scott, R.L., 2017. Impacts of hydraulic redistribution on grass–tree competition vs facilitation in a semi-arid savanna. New Phytol. 215, 1451–1461. https://doi.org/10.1111/nph.14693

Barron-Gafford, G.A., Scott, R.L., Jenerette, G.D., Hamerlynck, E.P., Huxman, T.E., 2013. Landscape and environmental controls over leaf and ecosystem carbon dioxide fluxes under woody plant expansion. J. Ecol. 101, 1471–1483.

Barron-Gafford, G.A., Scott, R.L., Jenerette, G.D., Hamerlynck, E.P., Huxman, T.E., 2012. Temperature and precipitation controls over leaf- and ecosystem-level CO2 flux along a woody plant encroachment gradient. Glob. Change Biol. 18, 1389–1400. https://doi.org/10.1111/j.1365-2486.2011.02599.x

Beringer, J., Moore, C.E., Cleverly, J., Campbell, D.I., Cleugh, H., De Kauwe, M.G., Kirschbaum, M.U.F., Griebel, A., Grover, S., Huete, A., Hutley, L.B., Laubach, J., Van Niel, T., Arndt, S.K., Bennett, A.C., Cernusak, L.A., Eamus, D., Ewenz, C.M., Goodrich, J.P., Jiang, M., Hinko-Najera, N., Isaac, P., Hobeichi, S., Knauer, J., Koerber, G.R., Liddell, M., Ma, X., Macfarlane, C., McHugh, I.D., Medlyn, B.E., Meyer, W.S., Norton, A.J., Owens, J., Pitman, A., Pendall, E., Prober, S.M., Ray, R.L., Restrepo-Coupe, N., Rifai, S.W., Rowlings, D., Schipper, L., Silberstein, R.P., Teckentrup, L., Thompson, S.E., Ukkola, A.M., Wall, A., Wang, Y.-P., Wardlaw, T.J., Woodgate, W., 2022. Bridge to the future: Important lessons from 20 years of ecosystem observations made by the OzFlux network. Glob. Change Biol. 28, 3489–3514. https://doi.org/10.1111/gcb.16141

778 Biederman, J.A., Scott, R.L., Arnone III, J.A., Jasoni, R.L., Litvak, M.E., Moreo, M.T., Papuga, S.A., Ponce-
779 Campos, G.E., Schreiner-McGraw, A.P., Vivoni, E.R., 2018. Shrubland carbon sink depends upon
780 winter water availability in the warm deserts of North America. Agric. For. Meteorol. 249, 407–
781 419. https://doi.org/10.1016/j.agrformet.2017.11.005
782 Biederman, J.A., Scott, R.L., Bell, T.W., Bowling, D.R., Dore, S., Garatuza-Payan, J., Kolb, T.E., Krishnan, P.,
783 Krofcheck, D.J., Litvak, M.E., Maurer, G.E., Meyers, T.P., Oechel, W.C., Papuga, S.A., Ponce-
784 Campos, G.E., Rodriguez, J.C., Smith, W.K., Vargas, R., Watts, C.J., Yepez, E.A., Goulden, M.L.,
785 2017. CO_2 exchange and evapotranspiration across dryland ecosystems of southwestern North
786 America. Glob. Change Biol. 23, 4204–4221. https://doi.org/10.1111/gcb.13686
787 Biederman, J.A., Scott, R.L., Goulden, M.L., Vargas, R., Litvak, M.E., Kolb, T.E., Yepez, E.A., Oechel, W.C.,
788 Blanken, P.D., Bell, T.W., Garatuza-Payan, J., Maurer, G.E., Dore, S., Burns, S.P., 2016. Terrestrial
789 carbon balance in a drier world: the effects of water availability in southwestern North America.
790 Glob. Change Biol. 22, 1867–1879. https://doi.org/10.1111/gcb.13222
791 Blyth, E.M., Arora, V.K., Clark, D.B., Dadson, S.J., De Kauwe, M.G., Lawrence, D.M., Melton, J.R.,
792 Pongratz, J., Turton, R.H., Yoshimura, K., Yuan, H., 2021. Advances in Land Surface Modelling.
793 Curr. Clim. Change Rep. 7, 45–71. https://doi.org/10.1007/s40641-021-00171-5
794 Browning, D.M., Karl, J.W., Morin, D., Richardson, A.D., Tweedie, C.E., 2017. Phenocams bridge the gap
795 between field and satellite observations in an arid grassland ecosystem. Remote Sens. 9, 1071.
796 https://doi.org/10.3390/rs9101071
797 Brust, C., Kimball, J.S., Maneta, M.P., Jencso, K., He, M., Reichle, R.H., 2021. Using SMAP Level-4 soil
798 moisture to constrain MOD16 evapotranspiration over the contiguous USA. Remote Sens.
799 Environ. 255, 112277. https://doi.org/10.1016/j.rse.2020.112277
800 Cable, D.R., 1975. Influence of precipitation on perennial grass production in the semidesert southwest.
801 Ecology 56, 981–986.
802 Cable, J.M., Barron-Gafford, G.A., Ogle, K., Pavao-Zuckerman, M., Scott, R.L., Williams, D.G., Huxman,
803 T.E., 2012. Shrub encroachment alters sensitivity of soil respiration to temperature and
804 moisture. J. Geophys. Res. - Biogeosciences 117, G01001.
805 https://doi.org/10.1029/2011JG001757
806 Cayan, D.R., Das, T., Pierce, D.W., Barnett, T.P., Tyree, M., Gershunov, A., 2010. Future dryness in the
807 southwest US and the hydrology of the early 21st century drought. Proc. Natl. Acad. Sci. 107,
808 21271–21276. https://doi.org/10.1073/pnas.0912391107
809 Chang, Q., Xiao, X., Wu, X., Doughty, R., Jiao, W., Bajgain, R., Qin, Y., Wang, J., 2020. Estimating site-
810 specific optimum air temperature and assessing its effect on the photosynthesis of grasslands in
811 mid-to high-latitudes. Environ. Res. Lett. 15, 034064. https://doi.org/10.1088/1748-
812 9326/ab70bb
813 Chu, H., Luo, X., Ouyang, Z., Chan, W.S., Dengel, S., Biraud, S.C., Torn, M.S., Metzger, S., Kumar, J., Arain,
814 M.A., 2021. Representativeness of Eddy-Covariance flux footprints for areas surrounding
815 AmeriFlux sites. Agric. For. Meteorol. 301, 108350.
816 Dannenberg, M.P., Barnes, M.L., Smith, W.K., Johnston, M.R., Meerdink, S.K., Wang, X., Scott, R.L.,
817 Biederman, J.A., 2023. Upscaling dryland carbon and water fluxes with artificial neural networks
818 of optical, thermal, and microwave satellite remote sensing. Biogeosciences 20, 383–404.
819 https://doi.org/10.5194/bg-20-383-2023
820 Desai, A.R., Murphy, B.A., Wiesner, S., Thom, J., Butterworth, B.J., Koupaei-Abyazani, N., Muttaqin, A.,
821 Paleri, S., Talib, A., Turner, J., Mineau, J., Merrelli, A., Stoy, P., Davis, K., 2022. Drivers of Decadal
822 Carbon Fluxes Across Temperate Ecosystems. J. Geophys. Res. Biogeosciences 127,
823 e2022JG007014. https://doi.org/10.1029/2022JG007014
824 Dufresne, J.-L., Foujols, M.-A., Denvil, S., Caubel, A., Marti, O., Aumont, O., Balkanski, Y., Bekki, S.,
825 Bellenger, H., Benshila, R., Bony, S., Bopp, L., Braconnot, P., Brockmann, P., Cadule, P., Cheruy,

F., Codron, F., Cozic, A., Cugnet, D., de Noblet, N., Duvel, J.-P., Ethé, C., Fairhead, L., Fichefet, T., Flavoni, S., Friedlingstein, P., Grandpeix, J.-Y., Guez, L., Guilyardi, E., Hauglustaine, D., Hourdin, F., Idelkadi, A., Ghattas, J., Joussaume, S., Kageyama, M., Krinner, G., Labetoulle, S., Lahellec, A., Lefebvre, M.-P., Lefevre, F., Levy, C., Li, Z.X., Lloyd, J., Lott, F., Madec, G., Mancip, M., Marchand, M., Masson, S., Meurdesoif, Y., Mignot, J., Musat, I., Parouty, S., Polcher, J., Rio, C., Schulz, M., Swingedouw, D., Szopa, S., Talandier, C., Terray, P., Viovy, N., Vuichard, N., 2013. Climate change projections using the IPSL-CM5 Earth System Model: from CMIP3 to CMIP5. Clim. Dyn. 40, 2123–2165. https://doi.org/10.1007/s00382-012-1636-1

El-Madany, T.S., Carrara, A., Martín, M.P., Moreno, G., Kolle, O., Pacheco-Labrador, J., Weber, U., Wutzler, T., Reichstein, M., Migliavacca, M., 2020. Drought and heatwave impacts on semi-arid ecosystems' carbon fluxes along a precipitation gradient. Philos. Trans. R. Soc. B Biol. Sci. 375, 20190519. https://doi.org/10.1098/rstb.2019.0519

Falge, E., Baldocchi, D., Olson, R., Anthoni, P., Aubinet, M., Bernhofer, C., Burba, G., Ceulemans, R., Clement, R., Dolman, H., Granier, A., Gross, P., Gru?nwald, T., Hollinger, D., Jensen, N.O., Katul, G., Keronen, P., Kowalski, A., Lai, C.T., Law, B.E., Meyers, T., Moncrieff, J., Moors, E., Munger, J.W., Pilegaard, K., Rannik, U., Rebmann, C., Suyker, A., Tenhunen, J., Tu, K., Verma, S., Vesala, T., Wilson, K., Wofsy, S., 2001. Gap filling strategies for defensible annual sums of net ecosystem exchange. Agric. For. Meteorol. 107, 43–69. https://doi.org/10.1016/S0168-1923(00)00225-2

Fawcett, D., Cunliffe, A.M., Sitch, S., O'Sullivan, M., Anderson, K., Brazier, R.E., Hill, T.C., Anthoni, P., Arneth, A., Arora, V.K., Briggs, P.R., Goll, D.S., Jain, A.K., Li, X., Lombardozzi, D., Nabel, J.E.M.S., Poulter, B., Séférian, R., Tian, H., Viovy, N., Wigneron, J.-P., Wiltshire, A., Zaehle, S., 2022. Assessing Model Predictions of Carbon Dynamics in Global Drylands. Front. Environ. Sci. 10. https://doi.org/10.3389/fenvs.2022.790200

Ficklin, D.L., Novick, K.A., 2017. Historic and projected changes in vapor pressure deficit suggest a continental-scale drying of the United States atmosphere. J. Geophys. Res. Atmospheres 122, 2061–2079. https://doi.org/10.1002/2016JD025855

Finzi, A.C., Giasson, M.-A., Barker Plotkin, A.A., Aber, J.D., Boose, E.R., Davidson, E.A., Dietze, M.C., Ellison, A.M., Frey, S.D., Goldman, E., Keenan, T.F., Melillo, J.M., Munger, J.W., Nadelhoffer, K.J., Ollinger, S.V., Orwig, D.A., Pederson, N., Richardson, A.D., Savage, K., Tang, J., Thompson, J.R., Williams, C.A., Wofsy, S.C., Zhou, Z., Foster, D.R., 2020. Carbon budget of the Harvard Forest Long-Term Ecological Research site: pattern, process, and response to global change. Ecol. Monogr. 90, e01423. https://doi.org/10.1002/ecm.1423

Friedlingstein, P., O'Sullivan, M., Jones, M.W., Andrew, R.M., Gregor, L., Hauck, J., Le Quéré, C., Luijkx, I.T., Olsen, A., Peters, G.P., Peters, W., Pongratz, J., Schwingshackl, C., Sitch, S., Canadell, J.G., Ciais, P., Jackson, R.B., Alin, S.R., Alkama, R., Arneth, A., Arora, V.K., Bates, N.R., Becker, M., Bellouin, N., Bittig, H.C., Bopp, L., Chevallier, F., Chini, L.P., Cronin, M., Evans, W., Falk, S., Feely, R.A., Gasser, T., Gehlen, M., Gkritzalis, T., Gloege, L., Grassi, G., Gruber, N., Gürses, Ö., Harris, I., Hefner, M., Houghton, R.A., Hurtt, G.C., Iida, Y., Ilyina, T., Jain, A.K., Jersild, A., Kadono, K., Kato, E., Kennedy, D., Klein Goldewijk, K., Knauer, J., Korsbakken, J.I., Landschützer, P., Lefèvre, N., Lindsay, K., Liu, J., Liu, Z., Marland, G., Mayot, N., McGrath, M.J., Metzl, N., Monacci, N.M., Munro, D.R., Nakaoka, S.-I., Niwa, Y., O'Brien, K., Ono, T., Palmer, P.I., Pan, N., Pierrot, D., Pocock, K., Poulter, B., Resplandy, L., Robertson, E., Rödenbeck, C., Rodriguez, C., Rosan, T.M., Schwinger, J., Séférian, R., Shutler, J.D., Skjelvan, I., Steinhoff, T., Sun, Q., Sutton, A.J., Sweeney, C., Takao, S., Tanhua, T., Tans, P.P., Tian, X., Tian, H., Tilbrook, B., Tsujino, H., Tubiello, F., van der Werf, G.R., Walker, A.P., Wanninkhof, R., Whitehead, C., Willstrand Wranne, A., Wright, R., Yuan, W., Yue, C., Yue, X., Zaehle, S., Zeng, J., Zheng, B., 2022. Global Carbon Budget 2022. Earth Syst. Sci. Data 14, 4811–4900. https://doi.org/10.5194/essd-14-4811-2022

873 Fu, Z., Li, D., Hararuk, O., Schwalm, C., Luo, Y., Yan, L., Niu, S., 2017. Recovery time and state change of
874 terrestrial carbon cycle after disturbance. Environ. Res. Lett. 12, 104004.
875 https://doi.org/10.1088/1748-9326/aa8a5c
876 Goodrich, D.C., Unkrich, C.L., Keefer, T.O., Nichols, M.H., Stone, J.J., Levick, L.R., Scott, R.L., 2008. Event
877 to multidecadal persistence in rainfall and runoff in southeast Arizona. Water Resour. Res. 44,
878 W05S14.
879 Goulden, M.L., Munger, J.W., Fan, S.M., Daube, B.C., Wofsy, S.C., 1996. Measurements of carbon
880 sequestration by long-term eddy covariance: Methods and a critical evaluation of accuracy.
881 Glob. Change Biol. 2, 169–182.
882 Hamerlynck, E.P., Scott, R.L., Moran, M.S., Keefer, T.O., Huxman, T.E., 2010. Growing season ecosystem
883 and leaf-level gas exchange of an exotic and native semiarid bunchgrass. Oecologia 163, 561–
884 570. https://doi.org/10.1007/s00442-009-1560-1
885 Hamerlynck, E.P., Scott, R.L., Stone, J.J., 2012. Soil moisture and ecosystem function responses of desert
886 grassland varying in vegetative cover to a saturating precipitation pulse. Ecohydrology 5, 297–
887 307. https://doi.org/10.1002/eco.214
888 Hastings, S.J., Oechel, W.C., Muhlia-Melo, A., 2005. Diurnal, seasonal and annual variation in the net
889 ecosystem CO2 exchange of a desert shrub community (Sarcocaulescent) in Baja California,
890 Mexico. Glob. Change Biol. 11, 927–939. https://doi.org/10.1111/j.1365-2486.2005.00951.x
891 Huang, J., Yu, H., Dai, A., Wei, Y., Kang, L., 2017. Drylands face potential threat under 2 °C global
892 warming target. Nat. Clim. Change 7, 417–422. https://doi.org/10.1038/nclimate3275
893 Huete, A., Didan, K., Miura, T., Rodriguez, E.P., Gao, X., Ferreira, L.G., 2002. Overview of the radiometric
894 and biophysical performance of the MODIS vegetation indices. Remote Sens. Environ. 83, 195–
895 213. https://doi.org/10.1016/S0034-4257(02)00096-2
896 Humphrey, V., Berg, A., Ciais, P., Gentine, P., Jung, M., Reichstein, M., Seneviratne, S.I., Frankenberg, C.,
897 2021. Soil moisture–atmosphere feedback dominates land carbon uptake variability. Nature
898 592, 65–69. https://doi.org/10.1038/s41586-021-03325-5
899 Hutley, L.B., O'Grady, A.P., Eamus, D., 2000. Evapotranspiration from Eucalypt open-forest savanna of
900 Northern Australia. Funct. Ecol. 14, 183–194. https://doi.org/10.1046/j.1365-2435.2000.00416.x
901 Huxman, T.E., Snyder, K.A., Tissue, D., Leffler, A.J., Ogle, K., Pockman, W.T., Sandquist, D.R., Potts, D.L.,
902 Schwinning, S., 2004. Precipitation pulses and carbon fluxes in semiarid and arid ecosystems.
903 Oecologia 141, 254–268. https://doi.org/10.1007/s00442-004-1682-4
904 Jenerette, G.D., Barron-Gafford, G.A., Guswa, A.J., McDonnell, J.J., Villegas, J.C., 2012. Organization of
905 complexity in water limited ecohydrology. Ecohydrology 5, 184–199.
906 https://doi.org/10.1002/eco.217
907 Joiner, J., Yoshida, Y., 2020. Satellite-based reflectances capture large fraction of variability in global
908 gross primary production (GPP) at weekly time scales. Agric. For. Meteorol. 291, 108092.
909 https://doi.org/10.1016/j.agrformet.2020.108092
910 Jones, L.A., Kimball, J.S., Reichle, R.H., Madani, N., Glassy, J., Ardizzone, J.V., Colliander, A., Cleverly, J.,
911 Desai, A.R., Eamus, D., 2017. The SMAP Level 4 Carbon Product for Monitoring Ecosystem Land–
912 Atmosphere CO 2 Exchange. IEEE Trans. Geosci. Remote Sens. 55, 6517–6532.
913 https://doi.org/10.1109/TGRS.2017.2729343
914 Keenan, T. f., Baker, I., Barr, A., Ciais, P., Davis, K., Dietze, M., Dragoni, D., Gough, C.M., Grant, R.,
915 Hollinger, D., Hufkens, K., Poulter, B., McCaughey, H., Raczka, B., Ryu, Y., Schaefer, K., Tian, H.,
916 Verbeeck, H., Zhao, M., Richardson, A.D., 2012. Terrestrial biosphere model performance for
917 inter-annual variability of land-atmosphere CO2 exchange. Glob. Change Biol. 18, 1971–1987.
918 https://doi.org/10.1111/j.1365-2486.2012.02678.x

Keenan, T.F., Hollinger, D.Y., Bohrer, G., Dragoni, D., Munger, J.W., Schmid, H.P., Richardson, A.D., 2013. Increase in forest water-use efficiency as atmospheric carbon dioxide concentrations rise. Nature 499, 324–327. https://doi.org/10.1038/nature12291

Keenan, T.F., Williams, C.A., 2018. The Terrestrial Carbon Sink. Annu. Rev. Environ. Resour. 43, 219–243. https://doi.org/10.1146/annurev-environ-102017-030204

Kemp, P.R., 1983. Phenological patterns of Chihuahuan desert plants in relation to the timing of water availability. J. Ecol. 71, 427–436. https://doi.org/10.2307/2259725

Knauer, J., Zaehle, S., Reichstein, M., Medlyn, B.E., Forkel, M., Hagemann, S., Werner, C., 2017. The response of ecosystem water-use efficiency to rising atmospheric CO2 concentrations: sensitivity and large-scale biogeochemical implications. New Phytol. 213, 1654–1666. https://doi.org/10.1111/nph.14288

Konings, A.G., Gentine, P., 2017. Global variations in ecosystem-scale isohydricity. Glob. Change Biol. 23, 891–905. https://doi.org/10.1111/gcb.13389

Krinner, G., Viovy, N., de Noblet-Ducoudré, N., Ogée, J., Polcher, J., Friedlingstein, P., Ciais, P., Sitch, S., Prentice, I.C., 2005. A dynamic global vegetation model for studies of the coupled atmosphere-biosphere system. Glob. Biogeochem. Cycles 19. https://doi.org/10.1029/2003GB002199

Kurc, S.A., Small, E.E., 2007. Soil moisture variations and ecosystem-scale fluxes of water and carbon in semiarid grassland and shrubland. Water Resour. Res. 43, W06416. https://doi.org/10.1029/2006WR005011

Lasslop, G., Reichstein, M., Papale, D., Richardson, A., Arneth, A., Barr, A., Stoy, P., Wohlfahrt, G., 2010. Separation of net ecosystem exchange into assimilation and respiration using a light response curve approach: Critical issues and global evaluation. Glob. Change Biol. 16, 187–208. https://doi.org/10.1111/j.1365-2486.2009.02041.x

Lee, E., Kumar, P., Barron-Gafford, G.A., Hendryx, S.M., Sanchez-Cañete, E.P., Minor, R.L., Colella, T., Scott, R.L., 2018. Impact of hydraulic redistribution on multispecies vegetation water use in a semiarid savanna ecosystem: An experimental and modeling synthesis. Water Resour. Res. 54, 4009–4027. https://doi.org/10.1029/2017WR021006

Liang, S., Cheng, J., Jia, K., Jiang, B., Liu, Q., Xiao, Z., Yao, Y., Yuan, W., Zhang, X., Zhao, X., Zhou, J., 2021. The Global Land Surface Satellite (GLASS) Product Suite. Bull. Am. Meteorol. Soc. 102, E323–E337. https://doi.org/10.1175/BAMS-D-18-0341.1

Ma, X., Huete, A., Cleverly, J., Eamus, D., Chevallier, F., Joiner, J., Poulter, B., Zhang, Y., Guanter, L., Meyer, W., 2016. Drought rapidly diminishes the large net CO2 uptake in 2011 over semi-arid Australia. Sci. Rep. 6, 37747. https://doi.org/10.1038/srep37747

Ma, X., Huete, A., Yu, Q., Coupe, N.R., Davies, K., Broich, M., Ratana, P., Beringer, J., Hutley, L.B., Cleverly, J., Boulain, N., Eamus, D., 2013. Spatial patterns and temporal dynamics in savanna vegetation phenology across the North Australian Tropical Transect. Remote Sens. Environ. 139, 97–115. https://doi.org/10.1016/j.rse.2013.07.030

MacBean, N., Scott, R.L., Biederman, J.A., Peylin, P., Kolb, T., Litvak, M.E., Krishnan, P., Meyers, T.P., Arora, V.K., Bastrikov, V., 2021. Dynamic global vegetation models underestimate net CO2 flux mean and inter-annual variability in dryland ecosystems. Environ. Res. Lett. 16, 094023. https://doi.org/10.1088/1748-9326/ac1a38

Mahmud, K., Raoult, N., Scott., R.L., MacBean, N., 2023. Data Assimilation as a Tool for Improving Seasonal Predictions of Evapotranspiration Partitioning in Southwestern US Semiarid Ecosystems. Prep.

Mahmud, K., Scott, R.L., Biederman, J.A., Litvak, M.E., Kolb, T., Meyers, T.P., Krishnan, P., Bastrikov, V., MacBean, N., 2021. Optimizing Carbon Cycle Parameters Drastically Improves Terrestrial Biosphere Model Underestimates of Dryland Mean Net CO2 Flux and its Inter-Annual Variability. J. Geophys. Res. Biogeosciences 126, e2021JG006400. https://doi.org/10.1029/2021JG006400

Martens, B., Gonzalez Miralles, D., Lievens, H., Van Der Schalie, R., De Jeu, R.A., Fernández-Prieto, D., Beck, H.E., Dorigo, W., Verhoest, N., 2017. GLEAM v3: Satellite-based land evaporation and root-zone soil moisture. Geosci. Model Dev. 10, 1903–1925. https://doi.org/10.5194/gmd-10-1903-2017

Melton, F.S., Huntington, J., Grimm, R., Herring, J., Hall, M., Rollison, D., Erickson, T., Allen, R., Anderson, M., Fisher, J.B., 2022. OpenET: Filling a critical data gap in water management for the western United States. JAWRA J. Am. Water Resour. Assoc. 58, 971–994. https://doi.org/10.1111/1752-1688.12956

Milly, P.C., Betancourt, J., Falkenmark, M., Hirsch, R.M., Kundzewicz, Z.W., Lettenmaier, D.P., Stouffer, R.J., 2008. Stationarity is dead: Whither water management? Science 319, 573–574. https://doi.org/10.1126/science.1151915

Miralles, D.G., Holmes, T.R.H., De Jeu, R. a. M., Gash, J.H., Meesters, A.G.C.A., Dolman, A.J., 2011. Global land-surface evaporation estimated from satellite-based observations. Hydrol. Earth Syst. Sci. 15, 453–469. https://doi.org/10.5194/hess-15-453-2011

Novick, K.A., Biederman, J.A., Desai, A.R., Litvak, M.E., Moore, D.J.P., Scott, R.L., Torn, M.S., 2018. The AmeriFlux network: A coalition of the willing. Agric. For. Meteorol. 249, 444–456. https://doi.org/10.1016/j.agrformet.2017.10.009

Novick, K.A., Ficklin, D.L., Baldocchi, D., Davis, K.J., Ghezzehei, T.A., Konings, A.G., MacBean, N., Raoult, N., Scott, R.L., Shi, Y., 2022. Confronting the water potential information gap. Nat. Geosci. 15, 158–164. https://doi.org/10.1038/s41561-022-00909-2

Novick, K.A., Ficklin, D.L., Stoy, P.C., Williams, C.A., Bohrer, G., Oishi, A.C., Papuga, S.A., Blanken, P.D., Noormets, A., Sulman, B.N., Scott, R.L., Wang, L., Philips, R.P., 2016. The increasing importance of atmospheric demand for ecosystem water and carbon fluxes. Nat. Clim. Change 6, 1023. https://doi.org/10.1038/nclimate3114

Pastorello, G., Trotta, C., Canfora, E., Chu, H., Christianson, D., Cheah, Y.-W., Poindexter, C., Chen, J., Elbashandy, A., Humphrey, M., Isaac, P., Polidori, D., Ribeca, A., van Ingen, C., Zhang, L., Amiro, B., Ammann, C., Arain, M.A., Ardö, J., Arkebauer, T., Arndt, S.K., Arriga, N., Aubinet, M., Aurela, M., Baldocchi, D., Barr, A., Beamesderfer, E., Marchesini, L.B., Bergeron, O., Beringer, J., Bernhofer, C., Berveiller, D., Billesbach, D., Black, T.A., Blanken, P.D., Bohrer, G., Boike, J., Bolstad, P.V., Bonal, D., Bonnefond, J.-M., Bowling, D.R., Bracho, R., Brodeur, J., Brümmer, C., Buchmann, N., Burban, B., Burns, S.P., Buysse, P., Cale, P., Cavagna, M., Cellier, P., Chen, S., Chini, I., Christensen, T.R., Cleverly, J., Collalti, A., Consalvo, C., Cook, B.D., Cook, D., Coursolle, C., Cremonese, E., Curtis, P.S., D'Andrea, E., da Rocha, H., Dai, X., Davis, K.J., De Cinti, B., de Grandcourt, A., De Ligne, A., De Oliveira, R.C., Delpierre, N., Desai, A.R., Di Bella, C.M., di Tommasi, P., Dolman, H., Domingo, F., Dong, G., Dore, S., Duce, P., Dufrêne, E., Dunn, A., Dušek, J., Eamus, D., Eichelmann, U., ElKhidir, H.A.M., Eugster, W., Ewenz, C.M., Ewers, B., Famulari, D., Fares, S., Feigenwinter, I., Feitz, A., Fensholt, R., Filippa, G., Fischer, M., Frank, J., Galvagno, M., Gharun, M., Gianelle, D., Gielen, B., Gioli, B., Gitelson, A., Goded, I., Goeckede, M., Goldstein, A.H., Gough, C.M., Goulden, M.L., Graf, A., Griebel, A., Gruening, C., Grünwald, T., Hammerle, A., Han, S., Han, X., Hansen, B.U., Hanson, C., Hatakka, J., He, Y., Hehn, M., Heinesch, B., Hinko-Najera, N., Hörtnagl, L., Hutley, L., Ibrom, A., Ikawa, H., Jackowicz-Korczynski, M., Janouš, D., Jans, W., Jassal, R., Jiang, S., Kato, T., Khomik, M., Klatt, J., Knohl, A., Knox, S., Kobayashi, H., Koerber, G., Kolle, O., Kosugi, Y., Kotani, A., Kowalski, A., Kruijt, B., Kurbatova, J., Kutsch, W.L., Kwon, H., Launiainen, S., Laurila, T., Law, B., Leuning, R., Li, Yingnian, Liddell, M., Limousin, J.-M., Lion, M., Liska, A.J., Lohila, A., López-Ballesteros, A., López-Blanco, E., Loubet, B., Loustau, D., Lucas-Moffat, A., Lüers, J., Ma, S., Macfarlane, C., Magliulo, V., Maier, R., Mammarella, I., Manca, G., Marcolla, B., Margolis, H.A., Marras, S., Massman, W., Mastepanov, M., Matamala, R., Matthes, J.H., Mazzenga, F., McCaughey, H., McHugh, I., McMillan, A.M.S., Merbold, L.,

Meyer, W., Meyers, T., Miller, S.D., Minerbi, S., Moderow, U., Monson, R.K., Montagnani, L., Moore, C.E., Moors, E., Moreaux, V., Moureaux, C., Munger, J.W., Nakai, T., Neirynck, J., Nesic, Z., Nicolini, G., Noormets, A., Northwood, M., Nosetto, M., Nouvellon, Y., Novick, K., Oechel, W., Olesen, J.E., Ourcival, J.-M., Papuga, S.A., Parmentier, F.-J., Paul-Limoges, E., Pavelka, M., Peichl, M., Pendall, E., Phillips, R.P., Pilegaard, K., Pirk, N., Posse, G., Powell, T., Prasse, H., Prober, S.M., Rambal, S., Rannik, Ü., Raz-Yaseef, N., Reed, D., de Dios, V.R., Restrepo-Coupe, N., Reverter, B.R., Roland, M., Sabbatini, S., Sachs, T., Saleska, S.R., Sánchez-Cañete, E.P., Sanchez-Mejia, Z.M., Schmid, H.P., Schmidt, M., Schneider, K., Schrader, F., Schroder, I., Scott, R.L., Sedlák, P., Serrano-Ortíz, P., Shao, C., Shi, P., Shironya, I., Siebicke, L., Šigut, L., Silberstein, R., Sirca, C., Spano, D., Steinbrecher, R., Stevens, R.M., Sturtevant, C., Suyker, A., Tagesson, T., Takanashi, S., Tang, Y., Tapper, N., Thom, J., Tiedemann, F., Tomassucci, M., Tuovinen, J.-P., Urbanski, S., Valentini, R., van der Molen, M., van Gorsel, E., van Huissteden, K., Varlagin, A., Verfaillie, J., Vesala, T., Vincke, C., Vitale, D., Vygodskaya, N., Walker, J.P., Walter-Shea, E., Wang, H., Weber, R., Westermann, S., Wille, C., Wofsy, S., Wohlfahrt, G., Wolf, S., Woodgate, W., Li, Yuelin, Zampedri, R., Zhang, J., Zhou, G., Zona, D., Agarwal, D., Biraud, S., Torn, M., Papale, D., 2020. The FLUXNET2015 dataset and the ONEFlux processing pipeline for eddy covariance data. Sci. Data 7, 225. https://doi.org/10.1038/s41597-020-0534-3

Pérez-Ruiz, E.R., Vivoni, E.R., Sala, O.E., 2022. Seasonal carryover of water and effects on carbon dynamics in a dryland ecosystem. Ecosphere 13, e4189. https://doi.org/10.1002/ecs2.4189

Petrie, M.D., Collins, S.L., Swann, A.M., Ford, P.L., Litvak, M.E., 2015. Grassland to shrubland state transitions enhance carbon sequestration in the northern Chihuahuan Desert. Glob. Change Biol. 21, 1226–1235.

Potts, D.L., Scott, R.L., Cable, J.E., Huxman, T.E., Williams, D.G., 2008. Sensitivity of mesquite shrubland CO2 exchange to precipitation in contrasting landscape settings. Ecology 89, 2900–2910. https://doi.org/10.1890/07-1177.1

Poulter, B., Frank, D., Ciais, P., Myneni, R.B., Andela, N., Bi, J., Broquet, G., Canadell, J.G., Chevallier, F., Liu, Y.Y., 2014. Contribution of semi-arid ecosystems to interannual variability of the global carbon cycle. Nature 509, 600–603.

Prentice, I.C., Liang, X., Medlyn, B.E., Wang, Y.-P., 2015. Reliable, robust and realistic: the three R's of next-generation land-surface modelling. Atmospheric Chem. Phys. 15, 5987–6005. https://doi.org/10.5194/acp-15-5987-2015

Reichstein, M., Falge, E., Baldocchi, D., Papale, D., Aubinet, M., Berbigier, P., Bernhofer, C., Buchmann, N., Gilmanov, T., Granier, A., Grunwald, T., Havrankova, K., Ilvesniemi, H., Janous, D., Knohl, A., Laurila, T., Lohila, A., Loustau, D., Matteucci, G., Meyers, T., Miglietta, F., Ourcival, J.M., Pumpanen, J., Rambal, S., Rotenberg, E., Sanz, M., Tenhunen, J., Seufert, G., Vaccari, F., Vesala, T., Yakir, D., Valentini, R., 2005. On the separation of net ecosystem exchange into assimilation and ecosystem respiration: Review and improved algorithm. Glob. Change Biol. 11, 1424–1439. https://doi.org/10.1111/j.1365-2486.2005.001002.x

Roby, M.C., Scott, R.L., Barron-Gafford, G.A., Hamerlynck, E.P., Moore, D.J.P., 2019. Environmental and vegetative controls on soil CO_2 efflux in three semiarid ecosystems. Soil Syst. 3, 6. https://doi.org/10.3390/soilsystems3010006

Roby, M.C., Scott, R.L., Biederman, J.A., Smith, W.K., Moore, D.J.P., 2022. Response of soil carbon dioxide efflux to temporal repackaging of rainfall into fewer, larger events in a semiarid grassland. Front. Environ. Sci. 10. https://doi.org/10.3389/fenvs.2022.940943

Roby, M.C., Scott, R.L., Moore, D.J.P., 2020. High Vapor Pressure Deficit Decreases the Productivity and Water Use Efficiency of Rain-Induced Pulses in Semiarid Ecosystems. J. Geophys. Res. Biogeosciences 125, e2020JG005665. https://doi.org/10.1029/2020JG005665

Running, S.W., Baldocchi, D.D., Turner, D.P., Gower, S.T., Bakwin, P.S., Hibbard, K.A., 1999. A global terrestrial monitoring network integrating tower fluxes, flask sampling, ecosystem modeling and EOS satellite data. Remote Sens. Environ. 70, 108–127. https://doi.org/10.1016/S0034-4257(99)00061-9

Running, S.W., Nemani, R.R., Heinsch, F.A., Zhao, M., Reeves, M., Hashimoto, H., 2004. A Continuous Satellite-Derived Measure of Global Terrestrial Primary Production. BioScience 54, 547–560. https://doi.org/10.1641/0006-3568(2004)054[0547:ACSMOG]2.0.CO;2

Schmid, H.P., 1997. Experimental design for flux measurements: Matching scales of observations and fluxes. Agric. For. Meteorol. 87, 179–200. https://doi.org/10.1016/S0168-1923(97)00011-7

Schwalm, C.R., Williams, C.A., Schaefer, K., Baldocchi, D., Black, T.A., Goldstein, A.H., Law, B.E., Oechel, W.C., Paw U, K.T., Scott, R.L., 2012. Reduction in carbon uptake during turn of the century drought in western North America. Nat. Geosci. 5, 551–556. https://doi.org/10.1038/ngeo1529

Scott, R.L., Biederman, J.A., 2019. Critical zone water balance over 13 years in a semiarid savanna. Water Resour. Res. 55, 574–588. https://doi.org/10.1029/2018WR023477

Scott, R.L., Biederman, J.A., 2017. Partitioning evapotranspiration using long-term carbon dioxide and water vapor fluxes. Geophys. Res. Lett. 44, 6833–6840. https://doi.org/10.1002/2017GL074324

Scott, R.L., Biederman, J.A., Hamerlynck, E.P., Barron-Gafford, G.A., 2015. The carbon balance pivot point of southwestern U.S. semiarid ecosystems: Insights from the 21st century drought. J. Geophys. Res. Biogeosciences 120, 2612–2624. https://doi.org/10.1002/2015JG003181

Scott, R.L., Cable, W.L., Hultine, K.R., 2008. The ecohydrologic significance of hydraulic redistribution in a semiarid savanna. Water Resour. Res. 44.

Scott, R.L., Jenerette, G.D., Potts, D.L., Huxman, T.E., 2009. Effects of seasonal drought on net carbon dioxide exchange from a woody-plant-encroached semiarid grassland. J. Geophys. Res. - Biogeosciences 114, G04004. https://doi.org/10.1029/2008JG000900

Shuttleworth, W.J., 1988. Evaporation from Amazonian rainforest. Proc. R. Soc. Lond. B Biol. Sci. 233, 321–346.

Smith, W.K., Biederman, J.A., Scott, R.L., Moore, D.J.P., He, M., Kimball, J.S., Yan, D., Hudson, A., Barnes, M.L., MacBean, N., Fox, A.M., Litvak, M.E., 2018. Chlorophyll Fluorescence Better Captures Seasonal and Interannual Gross Primary Productivity Dynamics Across Dryland Ecosystems of Southwestern North America. Geophys. Res. Lett. 748–757. https://doi.org/10.1002/2017GL075922

Steiner, B., 2022. Delayed Tree Dormancy Resulted in Higher Annual Savanna Gross Primary Productivity in the Northern Sonoran Desert (PhD Thesis). The University of Arizona.

Swain, D.L., Langenbrunner, B., Neelin, J.D., Hall, A., 2018. Increasing precipitation volatility in twenty-first-century California. Nat. Clim. Change 8, 427–433. https://doi.org/10.1038/s41558-018-0140-y

Tarin, T., Nolan, R.H., Eamus, D., Cleverly, J., 2020. Carbon and water fluxes in two adjacent Australian semi-arid ecosystems. Agric. For. Meteorol. 281, 107853. https://doi.org/10.1016/j.agrformet.2019.107853

Teckentrup, L., De Kauwe, M.G., Pitman, A.J., Goll, D.S., Haverd, V., Jain, A.K., Joetzjer, E., Kato, E., Lienert, S., Lombardozzi, D., McGuire, P.C., Melton, J.R., Nabel, J.E.M.S., Pongratz, J., Sitch, S., Walker, A.P., Zaehle, S., 2021. Assessing the representation of the Australian carbon cycle in global vegetation models. Biogeosciences 18, 5639–5668. https://doi.org/10.5194/bg-18-5639-2021

Unland, H.E., Houser, P.R., Shuttleworth, W.J., Yang, Z.L., 1996. Surface flux measurement and modeling at a semi-arid Sonoran Desert site. Agric. For. Meteorol. 82, 119–153. https://doi.org/10.1016/0168-1923(96)02330-1

Vivoni, E.R., Moreno, H.A., Mascaro, G., Rodriguez, J.C., Watts, C.J., Garatuza-Payan, J., Scott, R.L., 2008. Observed relation between evapotranspiration and soil moisture in the North American monsoon region. Geophys. Res. Lett. 35, L22403.

Vivoni, E.R., Pérez-Ruiz, E.R., Scott, R.L., Naito, A.T., Archer, S.R., Biederman, J.A., Templeton, N.P., 2022. A micrometeorological flux perspective on brush management in a shrub-encroached Sonoran Desert grassland. Agric. For. Meteorol. 313, 108763. https://doi.org/10.1016/j.agrformet.2021.108763

Walker, A.P., De Kauwe, M.G., Bastos, A., Belmecheri, S., Georgiou, K., Keeling, R.F., McMahon, S.M., Medlyn, B.E., Moore, D.J., Norby, R.J., 2021. Integrating the evidence for a terrestrial carbon sink caused by increasing atmospheric CO2. New Phytol. 229, 2413–2445. https://doi.org/10.1111/nph.16866

Wang, H., Li, X., Xiao, J., Ma, M., 2021. Evapotranspiration components and water use efficiency from desert to alpine ecosystems in drylands. Agric. For. Meteorol. 298–299, 108283. https://doi.org/10.1016/j.agrformet.2020.108283

Wang, X., Biederman, J.A., Knowles, J.F., Scott, R.L., Turner, A.J., Dannenberg, M.P., Köhler, P., Frankenberg, C., Litvak, M.E., Flerchinger, G.N., Law, B.E., Kwon, H., Reed, S.C., Parton, W.J., Barron-Gafford, G.A., Smith, W.K., 2022. Satellite solar-induced chlorophyll fluorescence and near-infrared reflectance capture complementary aspects of dryland vegetation productivity dynamics. Remote Sens. Environ. 270, 112858. https://doi.org/10.1016/j.rse.2021.112858

Whitley, R., Beringer, J., Hutley, L.B., Abramowitz, G., De Kauwe, M.G., Evans, B., Haverd, V., Li, L., Moore, C., Ryu, Y., Scheiter, S., Schymanski, S.J., Smith, B., Wang, Y.-P., Williams, M., Yu, Q., 2017. Challenges and opportunities in land surface modelling of savanna ecosystems. Biogeosciences 14, 4711–4732. https://doi.org/10.5194/bg-14-4711-2017

Williams, A.P., Cook, B.I., Smerdon, J.E., 2022. Rapid intensification of the emerging southwestern North American megadrought in 2020–2021. Nat. Clim. Change 12, 232–234. https://doi.org/10.1038/s41558-022-01290-z

Yan, D., Scott, R.L., Moore, D.J.P., Biederman, J.A., Smith, W.K., 2019. Understanding the relationship between vegetation greenness and productivity across dryland ecosystems through the integration of PhenoCam, satellite, and eddy covariance data. Remote Sens. Environ. 223, 50–62. https://doi.org/10.1016/j.rse.2018.12.029

Yao, Y., Liang, S., Li, X., Hong, Y., Fisher, J.B., Zhang, N., Chen, J., Cheng, J., Zhao, S., Zhang, X., Jiang, B., Sun, L., Jia, K., Wang, K., Chen, Y., Mu, Q., Feng, F., 2014. Bayesian multimodel estimation of global terrestrial latent heat flux from eddy covariance, meteorological, and satellite observations. J. Geophys. Res. Atmospheres 119, 4521–4545. https://doi.org/10.1002/2013JD020864

Yuan, W., Zheng, Y., Piao, S., Ciais, P., Lombardozzi, D., Wang, Y., Ryu, Y., Chen, G., Dong, W., Hu, Z., 2019. Increased atmospheric vapor pressure deficit reduces global vegetation growth. Sci. Adv. 5, eaax1396. https://doi.org/10.1126/sciadv.aax1396

Zhang, X., Wang, Y.-P., Peng, S., Rayner, P.J., Ciais, P., Silver, J.D., Piao, S., Zhu, Z., Lu, X., Zheng, X., 2018. Dominant regions and drivers of the variability of the global land carbon sink across timescales. Glob. Change Biol. 24, 3954–3968. https://doi.org/10.1111/gcb.14275

Zhou, L., Chen, H., Dai, Y., 2015. Stronger warming amplification over drier ecoregions observed since 1979. Environ. Res. Lett. 10, 064012. https://doi.org/2020031315122679

Zhou, S., Yu, B., Huang, Y., Wang, G., 2015. Daily underlying water use efficiency for AmeriFlux sites. J. Geophys. Res. Biogeosciences 120, 887–902. https://doi.org/10.1002/2015JG002947